Article

Current Biology

Evolution of crossover interference enables stable autopolyploidy by ensuring pairwise partner connections in *Arabidopsis arenosa*

Graphical abstract

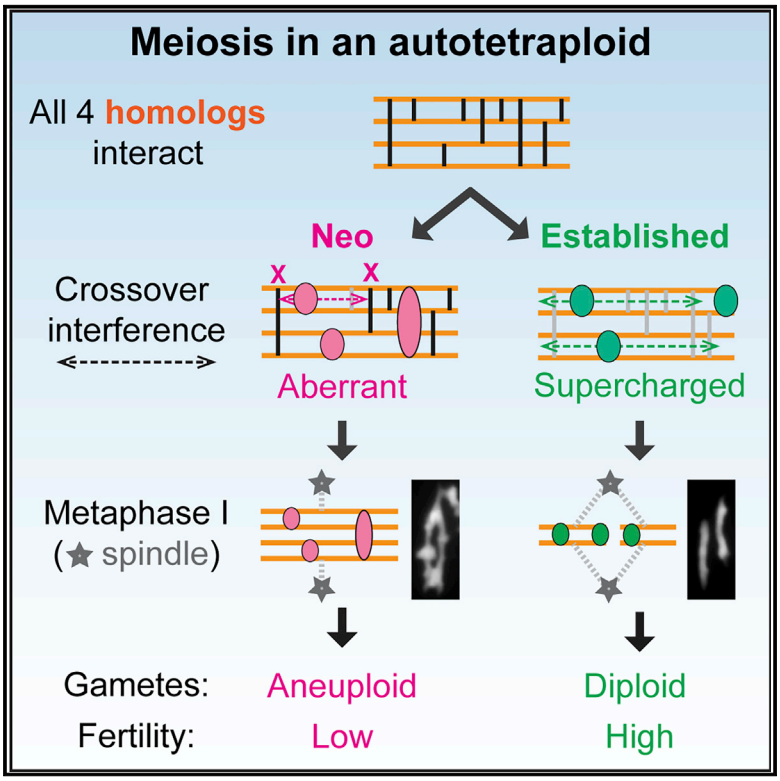

Authors

Chris Morgan, Martin A. White, F. Chris H. Franklin, Denise Zickler, Nancy Kleckner, Kirsten Bomblies

Correspondence

kleckner@fas.harvard.edu (N.K.), kirsten.bomblies@biol.ethz.ch (K.B.)

In brief

How does an established autopolyploid segregate its (multiple) homologous chromosomes two by two during meiosis? Morgan, White et al. show that crossover interference plays a critical role. They propose that stable autopolyploidy evolves by "supercharging" of interference and show that this also preadapts autotetraploid meiosis to higher ploidies.

Highlights

- In a neo-autotetraploid, aberrant crossover interference confers aberrant meiosis
- In a stable autotetraploid, regular crossover interference confers regular meiosis
- Crossover and synaptic patterns point to evolution of "supercharged" interference
- Accordingly, evolution of stable autotetraploidy preadapts to higher ploidies

Morgan et al., 2021, Current Biology *31*, 4713–4726
November 8, 2021
https://doi.org/10.1016/j.cub.2021.08.028

CellPress

Current Biology

CellPress
OPEN ACCESS

Article

Evolution of crossover interference enables stable autopolyploidy by ensuring pairwise partner connections in *Arabidopsis arenosa*

Chris Morgan,[1,6] Martin A. White,[2,6] F. Chris H. Franklin,[3] Denise Zickler,[4] Nancy Kleckner,[2,*] and Kirsten Bomblies[1,5,7,8,*]
[1]John Innes Centre, Colney Lane, Norwich NR4 7UH, UK
[2]Department of Molecular and Cellular Biology, Harvard University, 52 Oxford Street, Cambridge, MA 02138, USA
[3]School of Biosciences, University of Birmingham, Birmingham B15 2TT, UK
[4]University Paris-Saclay, Commissariat à l'Energie Atomique at aux Energies Alternatives (CEA), Centre National de la Recherche Scientifique (CNRS), Institute for Integrative Biology of the Cell (I2BC), 1 Avenue de la Terrasse, 91198 Gif-sur-Yvette, France
[5]Present address: Institute of Molecular Plant Biology, Department of Biology, ETH-Zürich, Universitätsstrasse 2, 8092 Zürich, Switzerland
[6]These authors contributed equally
[7]Twitter: @KBomblies
[8]Lead contact
*Correspondence: kleckner@fas.harvard.edu (N.K.), kirsten.bomblies@biol.ethz.ch (K.B.)
https://doi.org/10.1016/j.cub.2021.08.028

SUMMARY

Polyploidy is a major driver of evolutionary change. Autopolyploids, which arise by within-species whole-genome duplication, carry multiple nearly identical copies of each chromosome. This presents an existential challenge to sexual reproduction. Meiotic chromosome segregation requires formation of DNA crossovers (COs) between two homologous chromosomes. How can this outcome be achieved when more than two essentially equivalent partners are available? We addressed this question by comparing diploid, neo-autotetraploid, and established autotetraploid *Arabidopsis arenosa* using new approaches for analysis of meiotic CO patterns in polyploids. We discover that crossover interference, the classical process responsible for patterning of COs in diploid meiosis, is defective in the neo-autotetraploid but robust in the established autotetraploid. The presented findings suggest that, initially, diploid-like interference fails to act effectively on multivalent pairing and accompanying pre-CO recombination interactions and that stable autopolyploid meiosis can emerge by evolution of a "supercharged" interference process, which can now act effectively on such configurations. Thus, the basic interference mechanism responsible for simplifying CO patterns *along* chromosomes in diploid meiosis has evolved the capability to also simplify CO patterns *among* chromosomes in autopolyploids, thereby promoting bivalent formation. We further show that evolution of stable autotetraploidy preadapts meiosis to higher ploidy, which in turn has interesting mechanistic and evolutionary implications.

INTRODUCTION

Polyploids, which arise via genome duplication, are important in evolution.[1–4] Phenotypic novelty may confer an immediate advantage,[4,5] while increased genome complexity enables longer term adaptation, diversification, and speciation.[6–9] When polyploids first arise, fertility is often low, as most newly arisen ("neo")-polyploids show extensive chromosome mis-segregation during meiosis, the specialized cellular program that underlies gamete formation (e.g., Choudhary et al.[10] and Parra-Nunez et al.[11]). But this challenge can be overcome: stable polyploids with regular chromosome segregation and high fertility have evolved repeatedly (e.g., Grandont et al.,[12] Bomblies et al.,[13,14] Carvalho et al.,[15] Charpentier et al.,[16] Wolf et al.,[17] and Spoelhof et al.[18]).

The fundamental challenge to meiotic chromosome segregation in polyploids arises from their extra chromosome copies. In diploid meiosis, the two (maternal and paternal) copies of each chromosome (homologs) segregate from each other at the first meiotic division (metaphase I). This "reductional" segregation, a critical step in haploid gamete production, is ensured by pairwise physical connections between homologs, "chiasmata," which reflect combined effects of one or a few interhomolog DNA crossovers (COs) plus sister chromatid cohesion (Figures 1A– 1C, top).[19] In neo-polyploids, COs/chiasmata often link multiple partners and the resulting multivalents frequently mis-segregate at metaphase I.[14,20,21] Evolution of stable polyploidy thus comprises mechanisms that ensure that COs preferentially link pairs of homologs, despite the availability of more possible partners.

Two distinct types of polyploids, auto- and allopolyploids, likely represent extremes of a continuum.[1,3,20] Allopolyploids arise via hybridization coupled with genome duplication and contain recognizably distinct subgenomes. In evolved

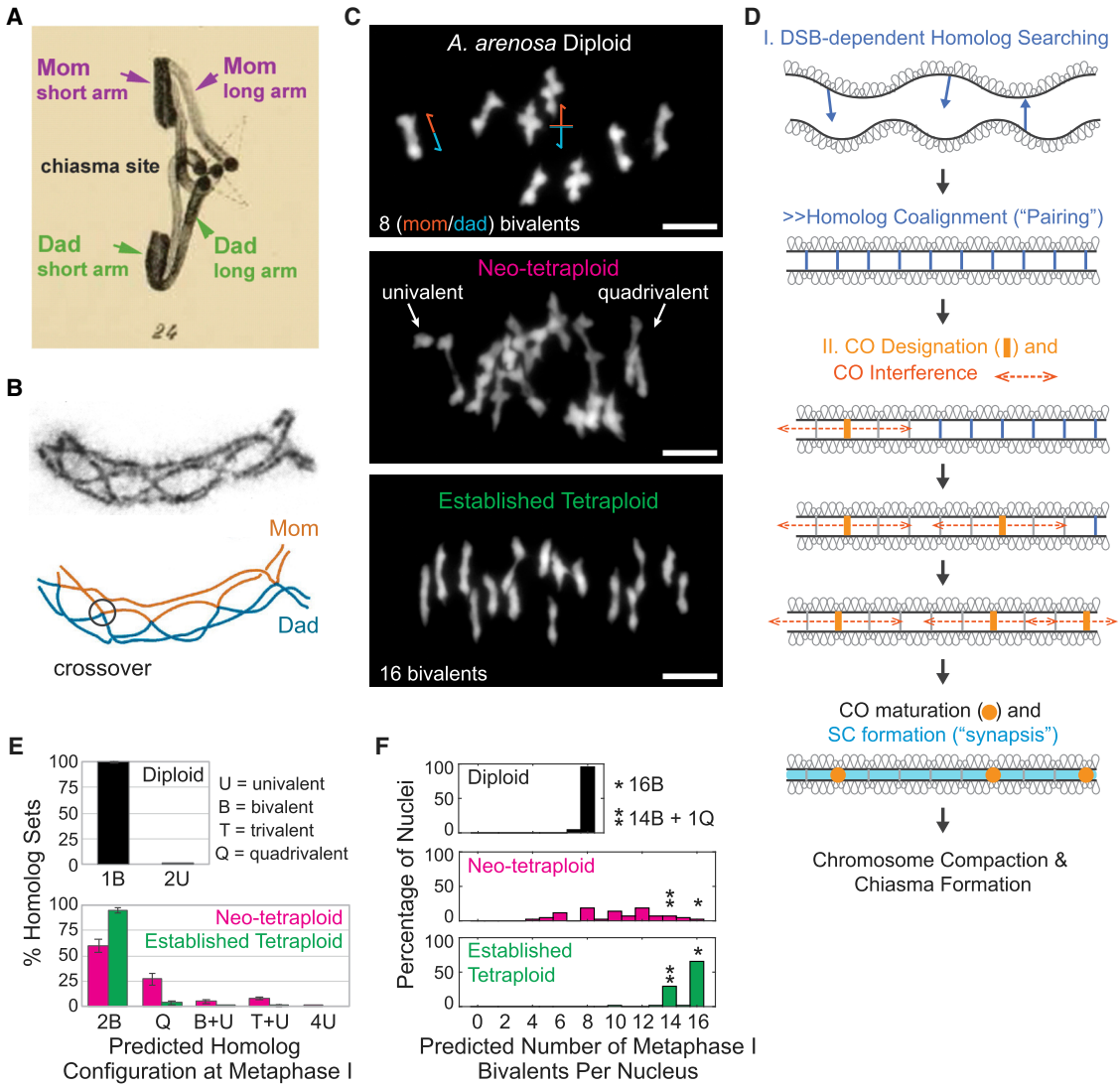

Figure 1. Metaphase I connections in diploid and autotetraploid nuclei

(A) Resolution of a chiasma at onset of anaphase[22] led to Janssens hypothesis that chiasmata represent sites of crossing over between homologs.

(B) Chromosome axes in grasshopper showing chiasmata (top) that correspond to sites of CO between homologs (bottom; adapted from Blat et al.[23]).

(C) Metaphase I chromosome complements in *A. arenosa* diploid, neo-tetraploid, and established tetraploid nuclei. Cartoons (top) show CO configurations corresponding to rod and cross-shaped bivalents. Scale bars, 5 μm.

(D) Initiation of recombination mediates homolog coalignment, which is followed by CO designation with accompanying CO interference and SC formation.

(E) Metaphase I configurations of total homolog sets (bivalents in diploids and quadrivalents in tetraploids) predicted from component homolog analysis as defined for *A. arenosa* diploid, neo-tetraploid, and established tetraploid nuclei. Error bars = standard error of the mean; n = 4 plants for diploid, neo-tetraploid, and established tetraploid.

(F) Percentages of nuclei exhibiting different numbers of bivalents predicted from component homolog analysis. In tetraploids, nuclei with 16 bivalents (*) and many nuclei with 14 bivalents and 1 quadrivalent (**) give regular metaphase I segregation (text). n = 90, 43, and 61 nuclei for diploid, neo-tetraploid, and established tetraploid, respectively.

See also Figures S2C and S3.

allopolyploids, and sometimes already in neo-allopolyploids, CO formation is restricted to more similar versions of each chromosome by mechanisms that recognize DNA sequence differences among subgenomes (e.g., Calderón et al.[24] and Henry et al.[25]). Autopolyploids arise by within-species whole-genome duplication, e.g., by fusion of unreduced gametes or mitotic errors. The multiple copies of each chromosome are thus equally homologous.[1,4,20,26] Correspondingly, when autopolyploids first form, COs generally occur promiscuously among all homologs, giving complex multivalent CO connections at metaphase I (e.g., Figure 1C, middle).[10,11,20,27] Neo-autopolyploids may thus be more prone to fertility defects arising from chromosome mis-segregation than neo-allopolyploids. Nonetheless, in most evolved autopolyploids, COs again link homologs primarily pairwise, without preferences for particular combinations, yielding diploid-like bivalents at metaphase I with stably polysomic

inheritance (e.g., Figure 1C, bottom).[17,27–31] Evolution of stable autopolyploidy is of special interest, because homolog copies must be recognized as pairs *qua* pairs, without cues from underlying genome sequence diversity.

We previously proposed that crossover interference might be important in autopolyploid meiotic stabilization.[14] Interference underlies patterning of COs in meiosis and, in diploids, arises as follows (Figure 1D). Recombination is initiated by programmed DNA double-strand breaks (DSBs), which occur in association with, and dependent upon, the chromosome structural axis.[32] At each DSB, one end identifies homologous DNA sequences on a partner homolog, and the resulting recombination complex establishes an interaction with this partner axis.[33] The two axes are then juxtaposed in space. Multiple DSBs thus yield coaligned homolog axes linked by multiple DSB-mediated recombination interactions.[33] COs then emerge at one or a few of these positions via a programmed patterning process. A first CO designation occurs, ensuring every homolog pair acquires at least one CO or chiasma (the so-called "obligatory CO" required for metaphase I segregation). That CO triggers a spreading interfering signal in both directions, dissipating with distance, that disfavors nearby CO designations. Interference spreads along chromosome axes over a distance defined in microns axis length.[34] Additional COs may then occur, with accompanying nucleation of an interfering signal, that "fill in the holes" between inhibitory domains created by prior events, leading to evenly spaced CO(s) along the chromosome, the classical outcome of crossover interference.[35] CO designation is accompanied by formation of the synaptonemal complex (SC), which is nucleated at a subset of pre-CO recombination interactions, likely all CO-designated sites, and additional interactions that mature to other fates.[35] Like COs or chiasmata, SC nucleations are evenly spaced and likely arise by the same process.[36]

To understand the evolution of stable autopolyploid meiosis, it is first necessary to understand the aberrant condition that occurs in neo-autopolyploids and then how evolution ultimately promotes regular pairwise CO connectedness in established autopolyploids. We developed ways of analyzing and comparing CO and SC patterns during meiosis in related diploid, neo-autotetraploid, and established autotetraploid *Arabidopsis arenosa*. This powerful system comprises a known founding diploid, from which neo-autotetraploids are easily generated, and a closely related meiotically stable autotetraploid that arose just once from a single ancestral population around 30,000 generations ago.[37] The natural (evolved) autotetraploid has stable bivalent formation,[15,38] without any tendency for chiasmata to occur preferentially between particular homolog pairs.[28] Also, a number of meiotic genes have been under selection in the autotetraploid lineage,[28,38,39] of which evolved alleles are associated with reduced multivalent formation rates.[40]

The present study uses 3D immunofluorescence structured illumination microscopy (SIM) to define positions of fluorescently tagged CO complexes along SCs. These CO positions provide a direct readout of the CO patterning process (above), permitting analysis of underlying mechanisms (e.g., Zhang et al.[34]). CO positions were analyzed with new approaches that allow extension of diploid methodologies to tetraploid meiosis. Diverse results support the hypothesis that CO interference plays a critical role in both the challenges of, and the solutions to, autotetraploid meiosis in *A. arenosa*. We also show that evolution of stable autotetraploidy preadapts meiosis to higher ploidy in this organism.

RESULTS

Cytological definition of synapsis patterns and CO positions

We defined CO patterns along SCs by immunocytological analysis in 194 diploid, neo-autotetraploid, and evolved autotetraploid *A. arenosa* male meiocytes (Figures 2 and S1; Video S1), isolated from 4 plants of each cytotype (STAR Methods). Quadrivalent synaptic configurations were observed in both neo- and established tetraploids, with continuous pairwise SCs along all four homolog copies and with component homologs switching partners at one or more positions ("synaptic partner switches" ["SPSs"]; Figure 2D). Quadrivalents with more than one SPS are rare (Figure S2). Neither trivalent or univalent nor non-homologous SC linkages were observed.

Pachytene quadrivalent configurations were computationally decomposed into their four individual component homologs. Within bivalents, or single SPS quadrivalents, paths of individual component homologs, and the positions of their COs, can be unambiguously defined (e.g., Figures 2D and 3A). The patterns of CO-mediated homolog connectedness that will emerge at metaphase I after loss of the SC can be predicted (Figure 3Ai).

We could now analyze CO patterns along component homologs (Figure 3Aii). Most component homologs exhibit only one or two COs. When two COs are present, these can be defined either as "two-homolog double COs," in which both COs of a reference chromosome are connected to the same partner, or "three-homolog double COs," in which the two COs of the reference chromosome are linked to two different partners. Importantly, three-homolog double COs result in multivalent metaphase I connectedness while two-homolog double COs do not (compare Figures 3Aii and 3Ai). The frequency of three-homolog double COs is much lower in the established tetraploid than in the neo-tetraploid (2% versus 20% of total component homologs; n = 1,952 and 1,376 component homologs). Categories of pachytene patterns observed for COs and SPSs, and their predicted metaphase I outcomes, are shown for 90 diploid, 43 neo-tetraploid, and 61 established tetraploid nuclei (Figure 3B).

Cytological inspection shows that, at metaphase I, diploids exhibit only bivalents; neo-tetraploids exhibit many complex "multivalents," reflecting promiscuous CO formation, and established tetraploids again exhibit primarily bivalents, reflecting restriction of COs to pairs of homologs (Figure 1C).[15,38] Quantitative analysis of metaphase I configurations predicted from component homolog analysis confirms these patterns (Figures 1E and S3). Furthermore, in the established tetraploid, more than 95% of nuclei should undergo regular segregation of all chromosomes (Figure 1F, bottom, asterisks): 66% exhibit 16 bivalents and 30% exhibit 14 bivalents plus 1 quadrivalent, which, in some orientations on the spindle, can undergo regular segregation. In the neo-tetraploid, very few nuclei exhibit one of these segregation-proficient configurations (2% and 7%, respectively; Figure 1F, middle, asterisks). These nuclei nonetheless provide a low level of fertility upon which selection could operate to give more favorable outcomes.[38]

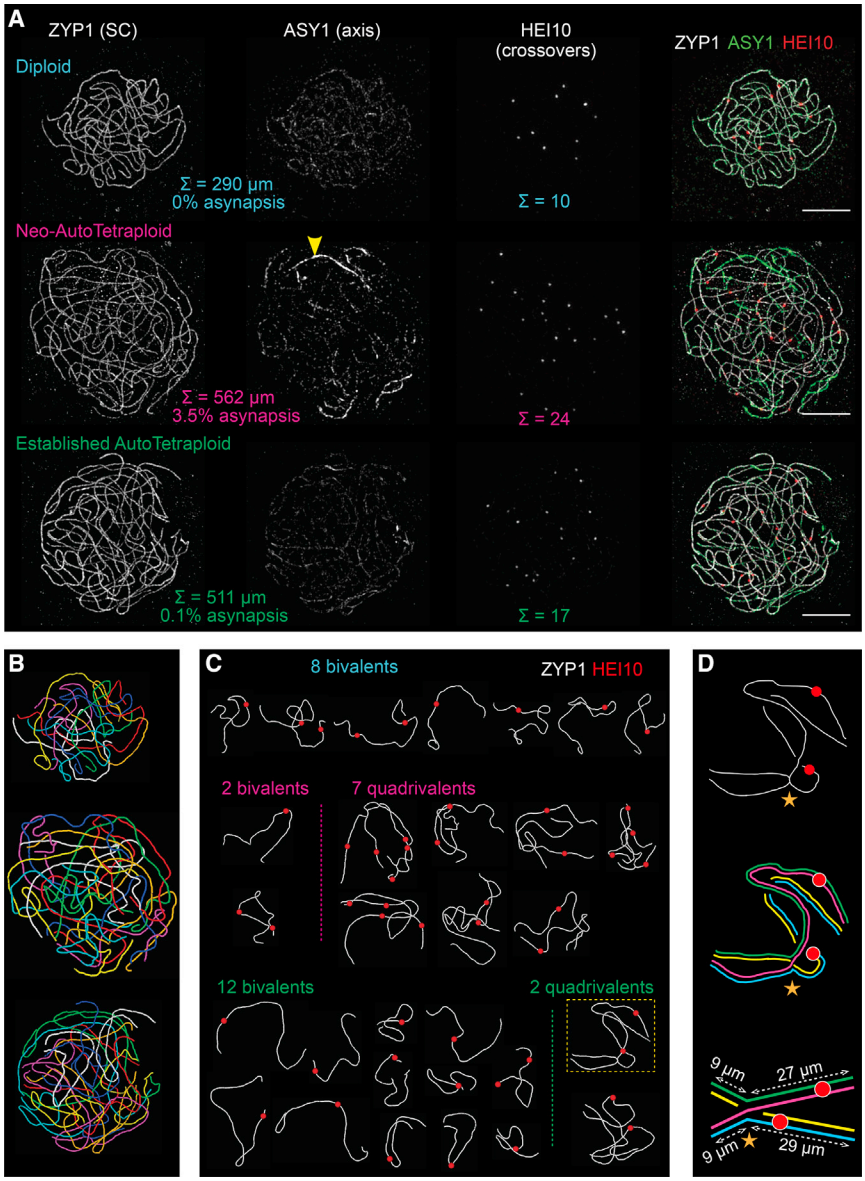

Figure 2. 3D immunofluorescence SIM images of *A. arenosa* diploid, neo-tetraploid, and established tetraploid late pachytene nuclei

(A) Mildly spread nuclei immunostained for indicated molecules to identify SCs (ZYP1), CO sites (HEI10), and axes (ASY1, where bright staining reveals asynapsis, yellow arrow, middle panel). Scale bars, 5 μm.

(B) Paths of all SCs of nuclei in (A) were computationally traced (colors arbitrary).

(C) SC paths (white) from the nuclei in (A) and (B) were segmented to identify individual bivalent and quadrivalent units, with positions of HEI10 foci (red) defined for each unit.

(D) Synaptic partner switch (SPS) for boxed quadrivalent in (C) (gold star, top), with component homologs identified (middle). Bottom: SPS is defined as a point where two SCs converge in 3D space with equal length arms.

See also Figure S1 and Video S1.

CO patterns in diploid, neo-autotetraploid, and established autotetraploid meiosis show that CO interference is important in tetraploid stabilization

CO interference was analyzed by classical coefficient of coincidence (CoC) analysis (Figures 4A and S4).[41] Each individual chromosome is divided into intervals. For each pair of intervals, the experimentally observed frequency of double COs (chromosomes with a CO in both intervals) is compared to the frequency expected if COs had occurred independently in the two intervals (the product of the frequencies of observed COs in each interval alone). The ratio of observed to expected double COs (the "CoC") is plotted as a function of inter-interval distance (in μm axis [SC] length; above).

Diploid *A. arenosa* exhibits defining features of meiotic CO interference. The CoC curve rises sigmoidally from a very low value to one over ~25 μm, the so-called "interference distance" (Figure 4A, top).[42] CO interference is also manifested in the distribution of distances between adjacent COs. This distribution is fit by a gamma distribution with a shape parameter (α) significantly greater than 1 (α = 5.8; Figure 4B, top), implying a tendency for even spacing (and thus interference, where α = 1 implies random [Poisson] distribution).

Importantly, the 25 μm distance over which CO interference spreads is a large proportion of the lengths of the eight *A. arenosa* chromosomes (mean 32 μm ± 6 μm standard deviation; Figure 4C, top). As a result, a first CO designation almost anywhere along a chromosome will establish interference that can extend along the entire remaining chromosome length, resulting in only a single CO per homolog. For longer chromosomes, a first CO designation near one chromosome end may still allow a second CO near the other end. Correspondingly, in *A. arenosa* diploids: (1) ~90% of chromosomes exhibit one CO and 10% exhibit two (Figure 4D, top); (2) COs on single-CO chromosomes are distributed centrally while COs on double CO chromosomes occur near the ends (Figure 4E, top); and (3) double COs are more common on longer chromosomes ($p = 3 \times 10^{-18}$, Wilcoxon rank-sum test; Figures 4F, top, and S4). Also, the frequency of zero-CO chromosomes is exceedingly low (Figure 4D, top), implying efficient occurrence of the obligatory CO.

Neo-autotetraploids exhibit compromised CO interference. In neo-tetraploid meiosis, the basic diploid-like interference process is still evident: (1) the CoC curve reaches a value of 1 at an inter-interval distance of ~18 μm, 72% of the ~25 μm in diploids (Figure 4A, middle); (2) the distribution of inter-CO distances is fit by a gamma distribution with $\alpha > 1$ (Figure 4B, middle); (3) the interference distance is still large relative to total chromosome lengths

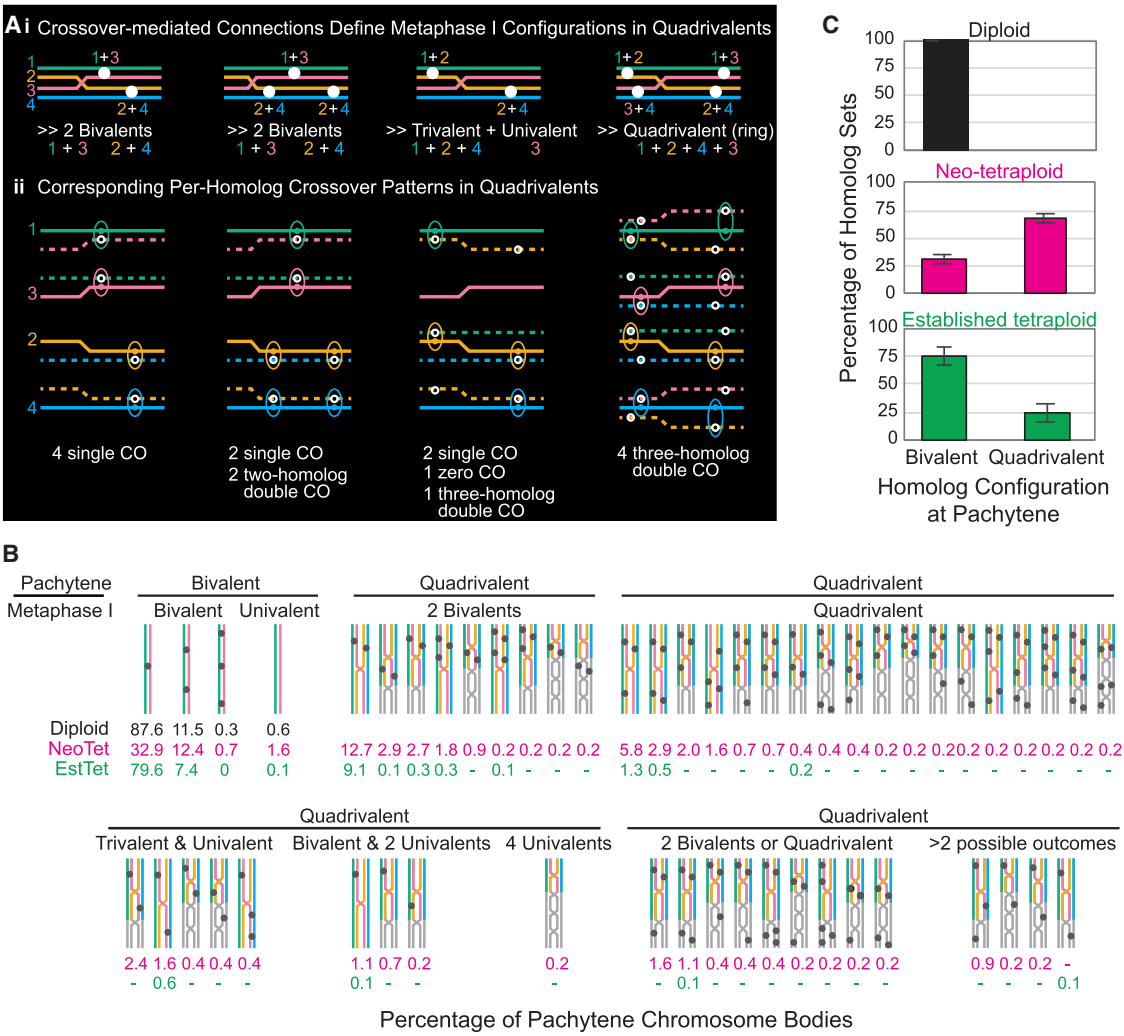

Figure 3. Component homolog analysis

(A) For quadrivalents with a single SPS, positions of COs along each of the four component homologs can be defined, enabling two analyses: (1) arrays of CO-mediated connections define the configurations that will occur at metaphase I, after loss of the SC. (2) For each individual component homolog copy, single, double, and occasional triple CO cases and corresponding CO positions can be identified and further analyzed, e.g., for CO interference.

(B) Frequencies of different CO and SPS patterns for all analyzed pachytene units. n = 720, 450, and 466 pachytene chromosome bodies for diploid, neo-tetraploid, and established tetraploid, respectively.

(C) Frequencies of different pachytene configurations in the three analyzed situations. Error bars show standard error of the mean. n = 4 plants for diploid, neo-tetraploid, and established tetraploid.

See also Figure S2.

(Figure 4C, middle), thus, most component homologs have only one CO (Figure 4D, middle); (4) COs on one-CO component homologs are still generally central, whereas COs on two-CO component homologs are positioned distally (Figure 4E, middle); and (5) one-CO component homologs tend to be shorter than those with more COs ($p = 3 \times 10^{-14}$, Wilcoxon rank-sum test; Figure 4F, middle). Zero-CO chromosomes are rare (Figure 4D, middle).

Nonetheless, CO interference is clearly compromised in neo-tetraploids. The CoC curve has elevated values at shorter inter-interval distances, implying double COs are more closely spaced than in the diploid (Figure 4A, middle versus top). Inter-CO distances are distributed around a lower median value than in the diploid (18 μm versus 22 μm; $p = 8 \times 10^{-8}$, Wilcoxon rank-sum test), and the best-fit gamma distribution shape parameter is lower than in the diploid ($\alpha = 4.9$ versus $\alpha = 5.8$), implying less even spacing (Figure 4B, middle versus top). In neo-tetraploids, 62% of component homologs have one CO (versus 90% in diploids), 30% have two, and 3% have three (Figure 4D, middle versus top). Finally, the tendencies for COs on one- and two-CO homologs to exhibit central versus distal positions is degraded compared to the diploid (Figure 4E, middle versus top). These effects are not attributable to the fact that neo-tetraploid chromosomes are slightly longer (33 μm versus 31 μm) than diploid chromosomes (Figure S5).

Established autotetraploid meiosis again exhibits robust CO interference. CO patterns in the established tetraploid are in nearly

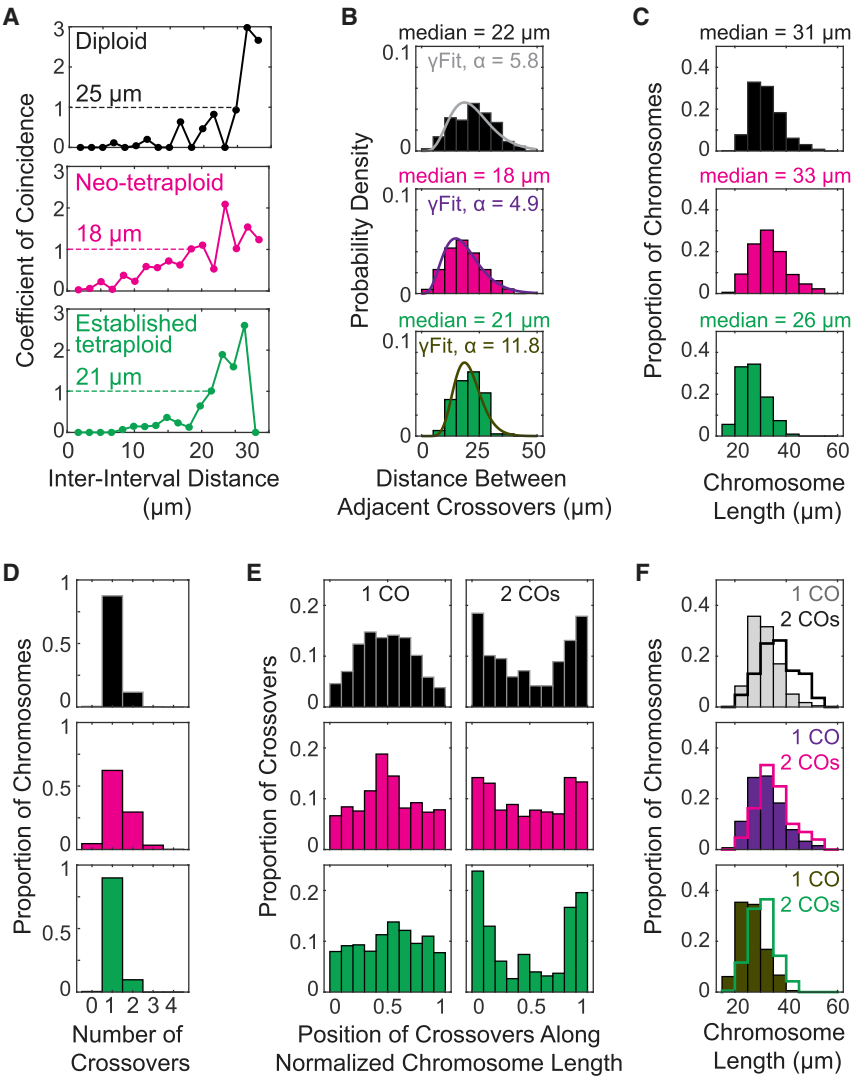

Figure 4. Crossover interference phenotypes

CO patterns in diploid and neo- and established tetraploids of *A. arenosa* as defined by component homolog analysis for all homologs in each case.

(A) Coefficient of coincidence (CoC).

(B) Inter-CO distance distribution plus shape parameter (α) of best-fit gamma distribution (γFit).

(C) Distribution of chromosome lengths.

(D) Distribution of numbers of COs per component homolog.

(E) Chromosomal positions of single and double COs (versus normalized chromosome length).

(F) Distributions of chromosome lengths for homologs with one or two COs.

For (A), n = 586, 486, and 622 component homologs between 27 and 33 μm in length for diploid, neo-tetraploid, and established tetraploid, respectively (STAR Methods). For (B), n = 176, 506, and 189 pairs of adjacent COs for diploid, neo-tetraploid, and established tetraploid, respectively. For (C) and (D), n = 1,440, 1,376, and 1,952 component homologs for diploid, neo-tetraploid, and established tetraploid, respectively. For (E) and (F), n = 1,260, 857, and 1,754 component homologs with a single CO and n = 168, 406, and 189 component homologs with a double CO for diploid, neo-tetraploid, and established tetraploid, respectively. See also Figures S2, S4, and S5.

all respects indistinguishable from patterns in diploids. CoC curves exhibit a sigmoidal shape, with little or no excess of closely spaced COs and with an interference distance of ~21 μm, 84% of the ~25 μm of the diploid (Figure 4A, bottom versus top). The distribution of inter-CO distances is centered on 21 μm, versus 22 μm in the diploid ($p = 0.009$, Wilcoxon rank-sum test) and 18 μm in the neo-tetraploid ($p = 4 \times 10^{-4}$, Wilcoxon rank-sum test), with a gamma distribution shape parameter of $\alpha = 12$ implying very robust even spacing (Figure 4B, bottom). As in diploids, 90% of component homologs exhibit only one CO (Figure 4D, bottom); COs in one-CO homologs are centrally located while COs in two-CO homologs are distally located, more strongly than in neo-tetraploids (Figure 4E, bottom); and chromosomes with one CO tend to be shorter than chromosomes with two COs ($p = 3 \times 10^{-24}$, Wilcoxon rank-sum test; Figure 4F, bottom). Zero-CO chromosomes are rare (Figure 4D, bottom). Overall, chromosomes are on average shorter in established tetraploids (26 μm) than diploids (31 μm) or neo-tetraploids (33 μm; $p = 3 \times 10^{-130}$ and 7×10^{-160}, respectively, Wilcoxon rank-sum test; Figure 4C). Although this allows greater effective spread of the interference signal as a proportion of chromosome length, neo-tetraploids exhibit an excess of COs over established tetraploids, even when chromosome length is controlled for (Figure S5).

Three scenarios for how CO interference might respond to multivalent pre-CO interactions

Tetraploids exhibit multivalent pre-CO coalignment. In principle, evolved polyploids might achieve pairwise CO or chiasma connectedness by regularizing partner selection at the coalignment stage, prior to and independent of CO patterning. However, this does not seem to be the case. Coalignment of multiple homolog axes is widely reported in both neo- and established auto- and allopolyploids (e.g., Grandont et al.,[12] Calderón et al.,[24] Loidl,[43] Jones and Vincent,[44] Rasmussen,[45] Stack and Roelofs,[46] and Humphrey[47]). In *A. arenosa*, the established tetraploid exhibits at least regional multivalent coalignment (Figures 5A and 5B) and larger scale effects are implied by coalignment of four homologs at later stages (Figures 5C and 5D).

Multivalent pre-CO coalignment presents a qualitatively new challenge to diploid-like CO interference: an interference signal nucleated by CO designation between one pair of homologs will initially spread along that pair but will sometimes encounter a junction at which one or both switch coalignment partners, engaging third or fourth homolog copies (Figure 5E, top). How does CO interference respond to such junctions? Could different responses in neo- and established tetraploids underlie their different CO patterns?

We can envision three scenarios (Figure 5E). In scenario 1, the spreading signal might ignore such junctions, giving regular CO

CellPress
OPEN ACCESS

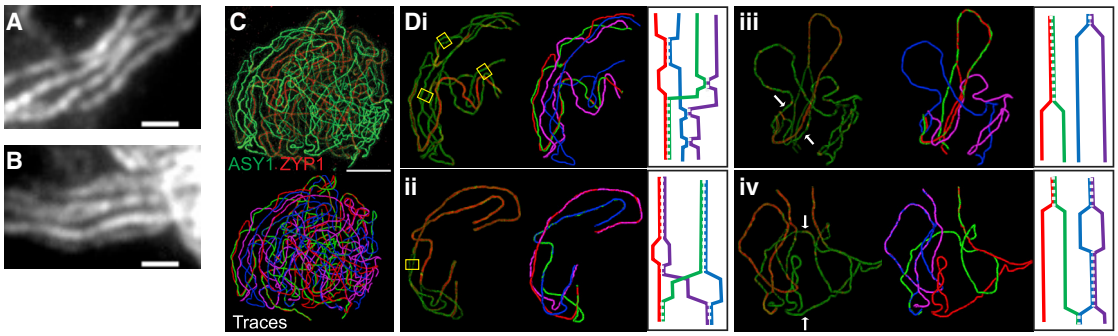

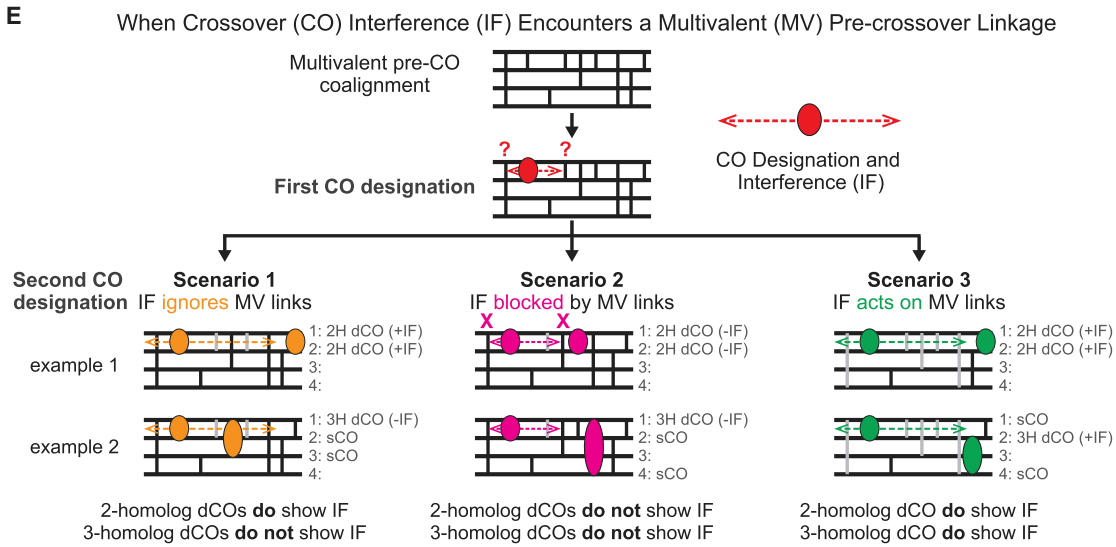

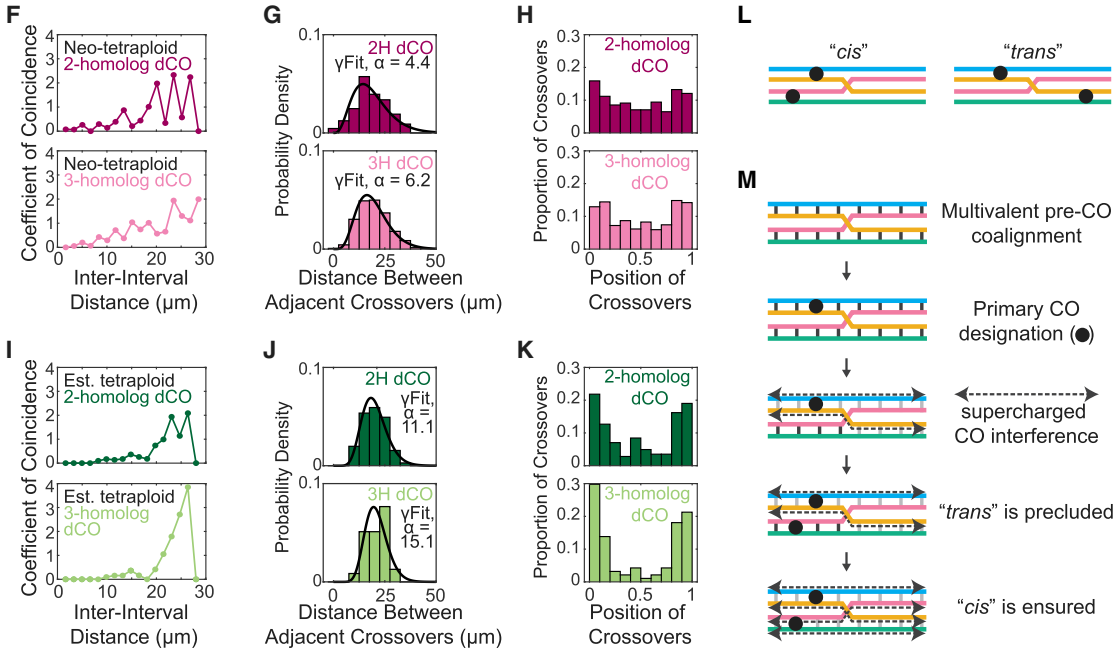

(legend on next page)

interference along the initiating pair without impacting interactions between the two initiating homologs and any third or fourth homolog (Figure 5E, left). In scenario 2, the spreading signal might be blocked at such junctions with its effect truncated along both members of the nucleating pair (Figure 5E, middle). In scenario 3, the spreading signal might act efficiently at such junctions, spreading along each of the individual nucleating homologs even if or after it switches coalignment partners; we call this "supercharged CO interference" (Figure 5E, right).

These three scenarios predict different patterns of two- and three-homolog double COs (Figure 5E, bottom and legend): in scenario 1, interference only affects the original nucleating pair, so two-homolog double COs will exhibit interference although three-homolog double COs will not. In scenario 2, both two- and three-homolog double COs will exhibit truncated interference (multivalent junctions affect both). In scenario 3, interference acts effectively across multivalent coalignment junctions so two- and three-homolog double COs will both exhibit robust interference.

Neo- and established autotetraploid CO phenotypes are explained by scenarios 2 and 3, respectively. In neo-autotetraploids, both two- and three-homolog double COs exhibit truncated interference as in scenario 2. CoC curves suggest an increase in closely spaced double COs, gamma distribution analysis suggests a decrease in evenness of CO spacing, and the positional difference between one- and two-CO homologs is degraded equivalently in both cases (Figures 5F–5H). In the established autotetraploid, both types of double COs exhibit robust interference as seen by sigmoidal CoC curves and restoration of even spacing as defined by the gamma distribution (Figures 5I–5K), as in scenario 3. Scenario 1 predictions are not observed in either autotetraploid. Three-homolog double CO patterns are particularly important because they must have arisen from multiply coaligned partners and are therefore specifically informative regarding effects in that context.

Additional support for this conclusion emerges from inspection of CO patterns in quadrivalents that exhibit two COs and a single SPS, where COs may occur on the same side of the SPS ("*cis*") or on opposite sides ("*trans*"; Figure 5L). The established tetraploid exhibits a strong bias toward the *cis* configuration compared to the neo-tetraploid (70.3% [n = 111] versus 24.3% [n = 235]; χ^2 [1 df; n = 346] = 71; $p < 0.01$). Supercharged CO interference in the established tetraploid explains these differences (Figure 5M). An SPS implies that a partner switch junction was present previously at the coalignment stage. Progression of interference through such a junction (scenario 3) will promote the *cis* outcome over *trans*.

Autotetraploid CO interference phenotypes are mirrored in SC or synapsis phenotypes

CO interference appears to be part of a broader interference process that results in even spacing of SC nucleation sites, a subset of which are (evenly spaced) COs.[36,48–52] In neo- and established tetraploids, interference among SC nucleations will be reflected in the spacing of adjacent SPS sites within pachytene quadrivalents (e.g., Figures 3B and 6A). By CoC analysis, adjacent SPSs exhibit interference in both tetraploids. However, just as for CO interference, SC nucleation and SPS interference is compromised in the neo-tetraploid, with an increased tendency for closely spaced double SPS sites and a lower average inter-SPS distance (Figures 6B and 6C). Reduced interference for SC nucleations also explains why the neo-tetraploid (versus the established tetraploid) exhibits a higher total frequency of pachytene quadrivalents (75% versus 25% of all "four homolog pachytene units"; Figure 3C) and more pachytene quadrivalents with two or more SPSs (46% versus 7%; n = 235 and 111 quadrivalents for neo-tetraploid and established tetraploid, respectively; Figure S6). Conversely, these observations provide direct evidence for interference-mediated SC nucleations in *Arabidopsis* as previously described in the fungus *Sordaria macrospora*.[36]

In diploid and established tetraploid pachytene nuclei, SC formation is continuous with very low levels of asynapsis (regions of bright ASY1 staining; Figures 2A, top and bottom, and 6D, left and right). In contrast, neo-tetraploids are asynapsed over 3%

Figure 5. Crossover interference in the context of multivalent pre-CO coalignment

(A and B) Regions where all four homolog copies are coaligned in parallel, prior to synapsis, are apparent in established tetraploids stained with axis component ASY1. Scale bars, 1 μm.

(C and D) Established tetraploid nucleus engaged in homolog juxtaposition illustrates global four-way coalignment and per-nucleus asynchrony.

(C) Whole nucleus stained for SC and axes (top) and the computationally traced paths of the 8 × 4 = 32 homolog axes (bottom).

(D) Selected four-homolog sets from (C). (i) and (ii) illustrate spatial juxtaposition of all four homologs along their lengths, despite synapsis, implying prior multivalent pre-SC coalignment. In (i)–(iv), different regions are at different stages of the juxtaposition process, including synapsis (e.g., red in left side of each panel) to distance coalignment at 4–700 nm (e.g., yellow boxes in i and ii) to very wide separation (e.g., white arrows at corresponding regions in iii and iv). Diagrams (right) are not to scale. Scale bars, 5 μm.

(E) If CO interference nucleated by CO designation involving one pair of homologs is operating within a multivalent pre-CO coalignment configuration, it will encounter recombination interactions that link one of the two nucleating homologs with a third or fourth homolog copy. The response to such encounters is not known (top). Three possible scenarios can be envisioned that make different predictions regarding whether two- and/or three-homolog double COs (2H dCOs; 3H dCOs) will or will not exhibit CO interference (+IF or −IF). Single CO homologs (sCO) will also occur in all cases.

(F–K) Comparison of 2H and 3H dCOs (top and bottom panels) with respect to various indicators of CO interference for neo-tetraploids (F–H) and established tetraploids (I–K).

(F and I) CoC analysis. n = 486 and 622 component homologs between 27 and 33 μm in length for neo-tetraploid and established tetraploid, respectively (STAR Methods).

(G and J) Inter-CO distance distribution plus shape parameter (α) of best-fit gamma distribution (γFit). No statistical difference was observed between the distributions for 2H and 3H dCOs ($p = 0.3$ and 0.2 for neo-tetraploid and established tetraploids, respectively; Wilcoxon rank sum test).

(H and K) Chromosomal positions of single and double COs (versus normalized chromosome length). For (G) and (H), n = 170 and 236 2H and 3H dCOs, and for (J) and (K), n = 142 and 47 2H and 3H dCOs, respectively.

(L) Pachytene quadrivalent configurations having two COs positioned in *cis* or in *trans* relative to a single SPS site.

(M) The *cis* and *trans* configurations in (L) will be favored and disfavored, respectively, by supercharged CO interference (scenario 3; E).

See also Figure S2G.

CellPress
OPEN ACCESS

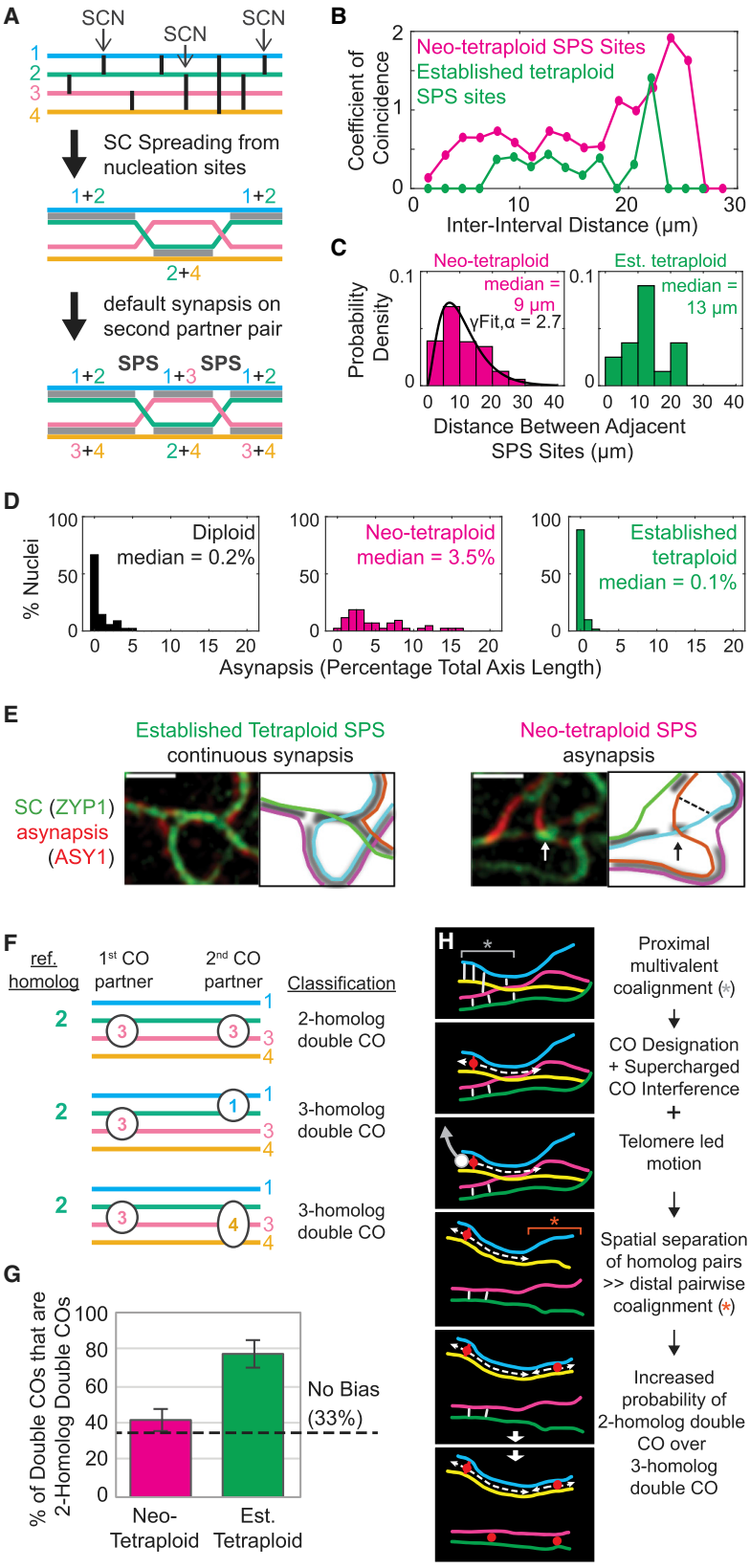

Figure 6. Synapsis patterns and dCO partner choice

(A) A pachytene SPS is generated when adjacent SC nucleations (SCNs) occur such that one common homolog has interacted with two different homolog partners. In this example, homolog 2 interacted with homologs 1, 4, and 1 at the three indicated SCNs. SC tends to spread outward from each SCN (M.W., unpublished data; gray bars, middle panel).[36] Opposite each SCN, synapsis involving the other partner pair will occur passively (additional gray bars, bottom panel). To the extent that SCN sites exhibit interference, so too will resulting SPSs.

(B and C) Analysis of SPSs in neo- and established tetraploid pachytene quadrivalents.

(B) Coefficient of coincidence analysis (n = 152 and 332 component homologs between 27 and 33 μm in length for neo-tetraploid and established tetraploid, respectively).

(C) Distribution of inter-SPS distances for neo- and established tetraploid quadrivalents. Best fit gamma distribution (γFit) and its shape parameter (α) are shown for the neo-tetraploid (n = 572); for the established tetraploid, sample size is too small for γFit (n = 32).

(D) Percentage of total axis length asynapsed at late pachytene. n = 90, 43, and 61 nuclei for diploid, neo-tetraploid, and established tetraploid, respectively.

(E) Left: SPS sites in established tetraploids exhibit continuous SC. Right: in neo-tetraploids, ~50% of SPS sites exhibit asynapsis (example shown); the remainder show continuous SC. Asynapsis could result from the presence of a residual pre-CO coalignment interaction that links two homologs. This interaction prevents the two linked homolog axes (arrow) from being drawn into different flanking SC segments (dashed line). Such an interaction is directly visible in this example because it nucleated a short segment of SC between the two linked axes (arrow; green staining). Scale bars, 1 μm.

(F) A reference homolog (2) gives a first CO by interaction with homolog (3) and then may give a second CO by interaction with any of the three available partners (1, 3, and 4), giving either a 2H dCO or a 3H dCO. If the partner for the second event is selected at random among the three possible homologs, the two outcomes will comprise 1/3 and 2/3 of all double COs, respectively.

(G) The proportion of 2H dCOs predicted for random dCO partner selection (33%) and observed for neo-tetraploids and established tetraploids. Error bars show standard error of the mean; n = 4 plants for both neo-tetraploid and established tetraploid. Data are for all measured component homologs (pachytene bivalents and quadrivalents) from each plant.

(H) Supercharged crossover interference nucleated by a CO at one chromosome end can promote distal pairwise pre-CO coalignment, thus promoting formation of a second CO at the other end between the same pair, yielding a 2H dCO (see also text).

See also Figure S6.

of total per-nucleus axis length (Figures 2A, middle, and 6D, middle). Strikingly, all asynaptic regions in neo-tetraploids (69 regions identified in a subset of 17 nuclei) occur at SPSs (e.g., Figure 6E, right) and 48% (69/144) of SPSs exhibit asynapsis. In contrast, in established tetraploid nuclei, all SPSs (119/119) exhibit continuous synapsis (e.g., Figure 6E, left). Thus, asynapsis at SPSs is a prominent, specific feature of neo-tetraploid meiosis. This phenotype is well explained by truncated CO interference at sites of multivalent coalignment junctions (scenario 2), where encountered junctions impede SC polymerization coming from flanking partner pairs (Figure 6E, right, dashed line). In some cases, unresolved interactions are directly visible because they nucleate a small internal SC segment at the site of the SPS (Figure 6E, right, arrow).

Double CO partner choice is random in neo-tetraploids and nonrandom in established tetraploids

If a particular homolog copy acquires two COs, these may both involve the same partner or different ones. If both COs choose partners independently, one-third of cases will involve the same partner and two-thirds will involve two partners. These two outcomes, manifested as two- and three-homolog double COs, would thus comprise 33% and 67% of total double COs, respectively (Figures 3Aii, 6F, and 6G). If a second CO preferentially selects the same partner as the first, there will be a bias toward two-homolog double COs.

The neo-tetraploid exhibits 39% and 61% two- and three-homolog double COs, respectively (Figure 6G). Thus, double CO partners are chosen essentially independently. This phenotype implies all three potential second CO partners are equally available, again providing strong evidence for multivalent pre-CO coalignment.

In contrast, the established tetraploid exhibits 75% and 25% two- and three-homolog double COs, respectively (Figure 6G), indicating coordinate formation of double COs along a given homolog pair. This is striking, given that the established tetraploid still exhibits multivalent coalignment (above). Supercharged CO interference can explain this paradox. When two COs occur, they tend to occur at opposite ends of the involved chromosome (above). Thus, when a first CO designation occurs between two homologs near one end, interference will spread toward the other end. This will release physical connections with third or fourth copies by directing recombination to the non-crossover fate[53] and/or by releasing recombination complexes from axes or SCs.[54] Ensuing SC formation will draw the involved homolog pair together, separating them from the third or fourth copies. Also, at this stage of meiotic prophase, dynamic telomere-led movements occur, which will move the involved homolog pair away from copies to which it is not connected.[55] Moreover, given overall chromosome stiffness, these effects will propagate toward distal regions. If those regions have not yet reached the coalignment stage, such coalignment and any second CO in this distal region will tend to involve the same pair of homologs as the first (Figure 6H). This effect requires that different regions of the genome are at different stages in the interhomolog interaction process. Indeed, per-nucleus asynchrony is a prominent feature of prophase in the established tetraploid (e.g., Figures 5C and 5D).[56,57]

Supercharged CO interference preadapts for meiosis at higher ploidy

Supercharged CO interference acts in *cis* along chromosomes and thus should operate on multivalent pre-CO coalignment configurations regardless of the number of associated copies, i.e., regardless of ploidy. We tested this idea by generating neo-auto-octoploids from the diploid and the established autotetraploid (Figure 7A). A neo-auto-octoploid created from a diploid exhibits even greater meiotic aberrations than the neo-autotetraploid: massive asynapsis at prophase and mostly multivalent associations at metaphase I (Figure 7B). In dramatic contrast, a neo-auto-octoploid created by whole-genome duplication of the established autotetraploid exhibits highly regular synapsis and almost exclusively bivalent configurations at metaphase I (Figure 7C). These findings suggest that supercharged CO interference in the established autotetraploid preadapts the genome for meiosis at higher ploidy.

DISCUSSION

The fundamental challenge for evolution of stable autopolyploid meiosis is achieving pairwise CO connectedness between homologs ("diploid-like metaphase I bivalent formation") despite the presence of more than two homologous copies of each chromosome. This process is especially interesting because it requires chromosome pairs to be recognized *qua* pairs, without input from genetic differences among potential partners (Introduction).

Here, we developed and applied a methodology for quantitative evaluation of CO interference, and SC nucleation interference in tetraploids, analyses not previously possible.[24,43–47] We focused on CO connectedness patterns rather than on effects that might simply reduce the number of COs (e.g., Pelé et al.[58]), because in principle, the number of COs does not matter if all COs occur between the same two homolog copies.

A pathway for the evolution of stable autopolyploid meiosis

We find that CO interference is compromised in *A. arenosa* neo-autotetraploids and robust in established autotetraploids. These and other observations suggest a particular scenario for the challenges to, and solutions for, stable autopolyploidy in this organism. In both autotetraploids, promiscuous DSB/partner interactions result in multivalent pre-CO recombination linkages at which the homolog(s) that nucleated the original signal switch partners to become coaligned with a third (fourth) homolog. In the neo-autotetraploid, diploid-like CO interference cannot cope with such junctions (scenario 2). This allows COs to occur among multiple partners, yielding mis-segregating multivalents at metaphase I. Stable autotetraploidy emerged by evolution of an enhanced (supercharged) interference activity, which can now act with equal effectiveness on all encountered interactions, even when nucleating homolog(s) switch to engage an additional homolog (scenario 3). Thus, COs almost exclusively link homologs in pairs, with very few multivalent associations. In essence, the fundamental process responsible for simplifying CO patterns *along* homologs in diploid meiosis has evolved a new activity that allows it to also simplify CO patterns *among* homologs. Analogous differences between the two types of autotetraploids are also observed for the more general process of SC nucleation interference.

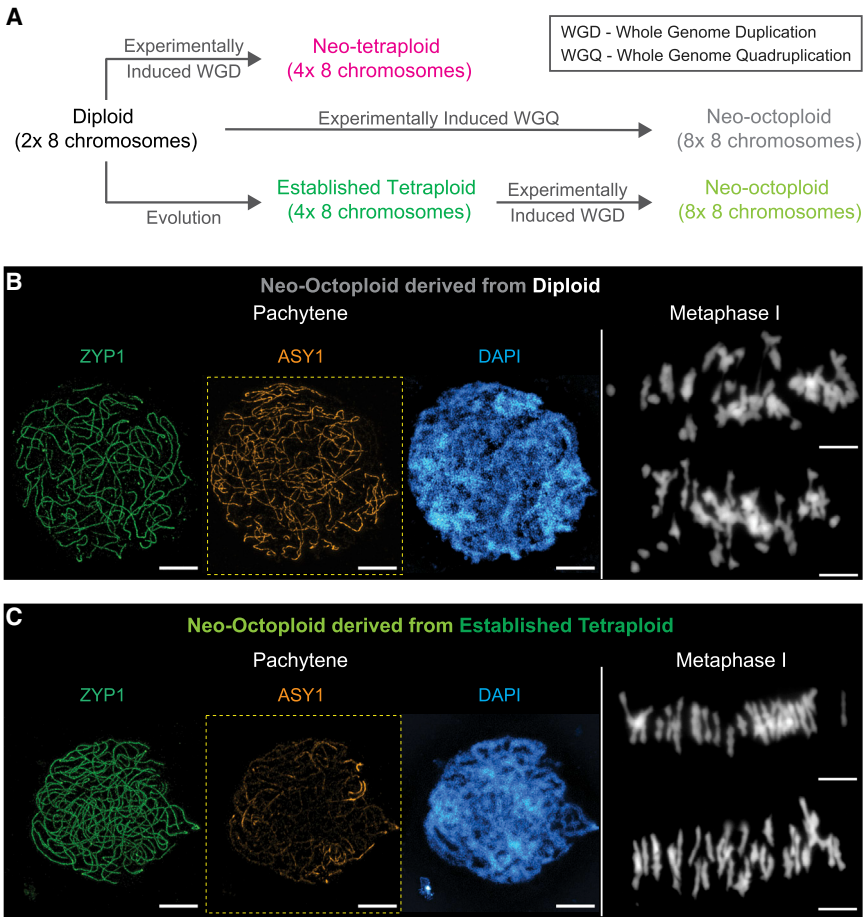

Figure 7. Neo-octoploids generated by whole-genome duplication

(A) Neo-octoploids were generated from diploids by two rounds of genome duplication and from established tetraploids by one round of genome duplication.

(B) Neo-octoploids derived from diploids exhibit high levels of asynapsis (ASY1, left) and massively aberrant non-bivalent metaphase I configurations (right). Scale bars, 5 μm.

(C) Neo-octoploids derived from established tetraploids exhibit regular synapsis and almost only bivalent metaphase I configurations (right). Scale bars, 5 μm.

Three additional findings are also of interest. First, CO interference acts over distances comparable to chromosome lengths in the progenitor diploid and both autotetraploids. Most importantly, this implies that, in the established autotetraploid, supercharged CO interference results in only one, occasionally two, COs along a given chromosome. Because the presence of only one CO automatically ensures pairwise CO connectedness at metaphase I, this effect dramatically minimizes opportunities for multivalent metaphase I CO connections. Second, in the established autotetraploid, an additional factor increases the probability that rare double COs tend to both engage the same partners, thus further reducing the frequency of multivalent interactions. This may be a secondary consequence of supercharged interference (above), implying that this process simplifies CO patterns by indirect as well as direct effects. Third, supercharged interference is predicted to be effective independent of ploidy. Accordingly, a diploid genome brought to a neo-auto-octoploid state has extensive asynapsis and produces many multivalents, while a neo-auto-octoploid generated from the established autotetraploid is very stable, showing near-complete synapsis and primarily bivalents in metaphase I.

Finally, we note that many species exhibit the basic features of meiotic interhomolog interactions described above for *A. arenosa* neo- and established autotetraploids (multivalent coalignment in both cases but simpler synaptic patterns and lower CO rates in established autotetraploids versus newly or less-established lines).[21] Thus, the progression proposed above for *A. arenosa* could be widely general.

Mechanism and molecular components of tetraploid meiotic adaptation

The biochemical mechanism of interference is not known, but considerable evidence suggests it spreads along chromosome axes.[42,59] Consistent with this possibility, several genes under selection in established *A. arenosa* autotetraploids[28,38,39] encode axis structure molecules: meiotic axis components ASY1 and ASY3;[60–62] PDS5, a general regulator of cohesin that can affect crossover patterns;[63,64] and REC8, a meiotic subunit of cohesin.[65] Even more interestingly, another gene under selection encodes PRD3, a homolog of Mer2, which is a major mediator of the recombination complex/axis interface and thus a potential target of interference.[66] Furthermore, derived alleles of ASY1 and ASY3 are associated with reduced multivalent formation in autotetraploids.[40] Another gene under selection is ZYP1, the transverse filament component of the SC, which is also required for normal CO interference.[52,67] It is not yet clear whether the requirement for ZYP1 comes into play before SC formation as in Sordaria[68] or via a role for the SC in spreading interference. The current analysis provides a new analytical framework for investigating effects of evolved alleles.

Preadaptation to higher ploidies

We show that evolution of stable autotetraploidy can preadapt meiosis for subsequent autopolyploidization. Interestingly, it was previously shown that duplication of the genome of an established *allo*tetraploid yielded an auto-octoploid that was *not* meiotically stable.[69] In allopolyploids, the solution to the problem of pairwise CO or chiasma connectedness relies on preferential CO formation between the two more similar copies of each chromosome.[25,70–76] This allotetraploid solution cannot provide preadaptation to subsequent autopolyploidization,

because genome doubling creates a novel situation in which each related pair of chromosomes (homeologs) is now present in multiple copies that cannot be distinguished by DNA sequence differences. By contrast, evolution of stable autotetraploidy via supercharged interference provides a mechanism that ensures pairwise interactions per se and thus among genetically near-identical copies. By extension, in nature, higher ploidy autopolyploids would be expected to more readily arise from pre-existing autotetraploids, whereas higher ploidy allopolyploids may have diverse origins.

STAR★METHODS

Detailed methods are provided in the online version of this paper and include the following:

- KEY RESOURCES TABLE
- RESOURCE AVAILABILITY
  - Lead contact
  - Materials availability
  - Data and code availability
- EXPERIMENTAL MODEL AND SUBJECT DETAILS
- METHOD DETAILS
  - Plant Material
  - Metaphase I Spreads
  - Immunocytology
- QUANTIFICATION AND STATISTICAL ANALYSIS
  - Sample Sizes
  - Defining synapsis patterns and CO positions
  - Component Homolog Generation
  - Coefficient of Coincidence Analysis

SUPPLEMENTAL INFORMATION

Supplemental information can be found online at https://doi.org/10.1016/j.cub.2021.08.028.

ACKNOWLEDGMENTS

This work was supported by a European Research Council Consolidator grant to K.B. (CoG EVO-MEIO 681946), the BBSRC via grant BB/P013511/1 to the John Innes Centre, an HFSP long-term fellowship to M.A.W. (LT000927/2013), and a grant from the NIH to N.K. (R35 GM136322).

AUTHOR CONTRIBUTIONS

Conceptualization, C.M., M.A.W., N.K., and K.B.; methodology, C.M., M.A.W., N.K., and K.B.; software, M.A.W.; formal analysis, C.M. and M.A.W.; investigation, C.M.; resources, F.C.H.F., N.K., and K.B.; writing – original draft, C.M., M.A.W., F.C.H.F., D.Z., N.K., and K.B.; writing – review & editing, C.M., M.A.W., F.C.H.F., D.Z., N.K., and K.B.; supervision, N.K. and K.B.; funding acquisition, N.K. and K.B.

DECLARATION OF INTERESTS

The authors declare no competing interests.

Received: March 29, 2021
Revised: July 23, 2021
Accepted: August 9, 2021
Published: September 3, 2021

REFERENCES

1. Otto, S.P., and Whitton, J. (2000). Polyploid incidence and evolution. Annu. Rev. Genet. *34*, 401–437.
2. Soltis, P.S., Liu, X., Marchant, D.B., Visger, C.J., and Soltis, D.E. (2014). Polyploidy and novelty: Gottlieb's legacy. Philos. Trans. R. Soc. Lond. B Biol. Sci. *369*, 20130351.
3. Ramsey, J., and Schemske, D.W. (1998). Pathways, mechanisms, and rates of polyploid formation in flowering plants. Annu. Rev. Ecol. Syst. *29*, 467–501.
4. Ramsey, J., and Schemske, D.W. (2002). Neopolyploidy in flowering plants. Annu. Rev. Ecol. Syst. *33*, 589–639.
5. Comai, L. (2005). The advantages and disadvantages of being polyploid. Nat. Rev. Genet. *6*, 836–846.
6. Arrigo, N., and Barker, M.S. (2012). Rarely successful polyploids and their legacy in plant genomes. Curr. Opin. Plant Biol. *15*, 140–146.
7. Soltis, D.E., Soltis, P.S., Bennett, M.D., and Leitch, I.J. (2003). Evolution of genome size in the angiosperms. Am. J. Bot. *90*, 1596–1603.
8. Fawcett, J.A., and Van de Peer, Y. (2010). Angiosperm polyploids and their road to evolutionary success. Trends Evol. Biol. *2*, e3.
9. Rieseberg, L.H., and Willis, J.H. (2007). Plant speciation. Science *317*, 910–914.
10. Choudhary, A., Wright, L., Ponce, O., Chen, J., Prashar, A., Sanchez-Moran, E., Luo, Z., and Compton, L. (2020). Varietal variation and chromosome behaviour during meiosis in Solanum tuberosum. Heredity *125*, 212–226.
11. Parra-Nunez, P., Pradillo, M., and Santos, J.L. (2019). Competition for chiasma formation between identical and homologous (but not identical) chromosomes in synthetic autotetraploids of *Arabidopsis thaliana*. Front. Plant Sci. *9*, 1924.
12. Grandont, L., Jenczewski, E., and Lloyd, A. (2013). Meiosis and its deviations in polyploid plants. Cytogenet. Genome Res. *140*, 171–184.
13. Bomblies, K., Higgins, J.D., and Yant, L. (2015). Meiosis evolves: adaptation to external and internal environments. New Phytol. *208*, 306–323.
14. Bomblies, K., Jones, G., Franklin, C., Zickler, D., and Kleckner, N. (2016). The challenge of evolving stable polyploidy: could an increase in "crossover interference distance" play a central role? Chromosoma *125*, 287–300.
15. Carvalho, A., Delgado, M., Barão, A., Frescatada, M., Ribeiro, E., Pikaard, C.S., Viegas, W., and Neves, N. (2010). Chromosome and DNA methylation dynamics during meiosis in the autotetraploid Arabidopsis arenosa. Sex. Plant Reprod. *23*, 29–37.
16. Charpentier, A., Feldman, M., and Cauderon, Y. (1986). Genetic control of meiotic chromosome pairing in tetraploid *Agropyron elongatum*. I. Pattern of pairing in natural and induced tetraploids and in F_1 triploid hybrids. Can. J. Genet. Cytol. *28*, 783–788.
17. Wolf, P.G., Soltis, P.S., and Soltis, D.E. (1989). Tetrasomic inheritance and chromosome pairing behaviour in the naturally occurring autotetraploid Heuchera grossulariifolia (Saxifragaceae). Genome *32*, 655–659.
18. Spoelhof, J.P., Chester, M., Rodriguez, R., Geraci, B., Heo, K., Mavrodiev, E., Soltis, P.S., and Soltis, D.E. (2017). Karyotypic variation and pollen stainability in resynthesized allopolyploids Tragopogon miscellus and T. mirus. Am. J. Bot. *104*, 1484–1492.
19. Zickler, D., and Kleckner, N. (1999). Meiotic chromosomes: integrating structure and function. Annu. Rev. Genet. *33*, 603–754.
20. Bomblies, K., and Madlung, A. (2014). Polyploidy in the Arabidopsis genus. Chromosome Res. *22*, 117–134.
21. Cifuentes, M., Grandont, L., Moore, G., Chèvre, A.M., and Jenczewski, E. (2010). Genetic regulation of meiosis in polyploid species: new insights into an old question. New Phytol. *186*, 29–36.
22. Koszul, R., Meselson, M., Van Doninck, K., Vandenhaute, J., and Zickler, D. (2012). The centenary of Janssens's chiasmatype theory. Genetics *191*, 309–317.

23. Blat, Y., Protacio, R.U., Hunter, N., and Kleckner, N. (2002). Physical and functional interactions among basic chromosome organizational features govern early steps of meiotic chiasma formation. Cell *111*, 791–802.

24. Calderón, M.C., Rey, M.D., Martín, A., and Prieto, P. (2018). Homoeologous chromosomes from two *Hordeum* species can recognize and associate during meiosis in wheat in the presence of the *Ph1* locus. Front. Plant Sci. *9*, 585.

25. Henry, I.M., Dilkes, B.P., Tyagi, A., Gao, J., Christensen, B., and Comai, L. (2014). The BOY NAMED SUE quantitative trait locus confers increased meiotic stability to an adapted natural allopolyploid of Arabidopsis. Plant Cell *26*, 181–194.

26. Parisod, C., Holderegger, R., and Brochmann, C. (2010). Evolutionary consequences of autopolyploidy. New Phytol. *186*, 5–17.

27. Santos, J.L., Alfaro, D., Sanchez-Moran, E., Armstrong, S.J., Franklin, F.C., and Jones, G.H. (2003). Partial diploidization of meiosis in autotetraploid Arabidopsis thaliana. Genetics *165*, 1533–1540.

28. Hollister, J.D., Arnold, B.J., Svedin, E., Xue, K.S., Dilkes, B.P., and Bomblies, K. (2012). Genetic adaptation associated with genome-doubling in autotetraploid Arabidopsis arenosa. PLoS Genet. *8*, e1003093.

29. Fjellstrom, R.G., Beuselinck, P.R., and Steiner, J.J. (2001). RFLP marker analysis supports tetrasonic inheritance in *Lotus corniculatus L*. Theor. Appl. Genet. *102*, 718–725.

30. Krebs, S.L., and Hancock, J.F. (1989). Tetrasomic inheritance of isoenzyme markers in the highbush blueberry, *Vaccinium corymbosum* L. Heredity *63*, 11–18.

31. Soltis, D.E., and Rieseberg, L.H. (1986). Autopolyploidy in Tolmiea menziesii (Saxifragaceae): genetic insights from enzyme electrophoresis. Am. J. Bot. *73*, 310–318.

32. Panizza, S., Mendoza, M.A., Berlinger, M., Huang, L., Nicolas, A., Shirahige, K., and Klein, F. (2011). Spo11-accessory proteins link double-strand break sites to the chromosome axis in early meiotic recombination. Cell *146*, 372–383.

33. Storlazzi, A., Gargano, S., Ruprich-Robert, G., Falque, M., David, M., Kleckner, N., and Zickler, D. (2010). Recombination proteins mediate meiotic spatial chromosome organization and pairing. Cell *141*, 94–106.

34. Zhang, L., Wang, S., Yin, S., Hong, S., Kim, K.P., and Kleckner, N. (2014). Topoisomerase II mediates meiotic crossover interference. Nature *511*, 551–556.

35. Wang, S., Zickler, D., Kleckner, N., and Zhang, L. (2015). Meiotic crossover patterns: obligatory crossover, interference and homeostasis in a single process. Cell Cycle *14*, 305–314.

36. Zhang, L., Espagne, E., de Muyt, A., Zickler, D., and Kleckner, N.E. (2014). Interference-mediated synaptonemal complex formation with embedded crossover designation. Proc. Natl. Acad. Sci. USA *111*, E5059–E5068.

37. Arnold, B., Kim, S.T., and Bomblies, K. (2015). Single geographic origin of a widespread autotetraploid Arabidopsis arenosa lineage followed by interploidy admixture. Mol. Biol. Evol. *32*, 1382–1395.

38. Yant, L., Hollister, J.D., Wright, K.M., Arnold, B.J., Higgins, J.D., Franklin, F.C.H., and Bomblies, K. (2013). Meiotic adaptation to genome duplication in Arabidopsis arenosa. Curr. Biol. *23*, 2151–2156.

39. Wright, K.M., Arnold, B., Xue, K., Šurinová, M., O'Connell, J., and Bomblies, K. (2015). Selection on meiosis genes in diploid and tetraploid Arabidopsis arenosa. Mol. Biol. Evol. *32*, 944–955.

40. Morgan, C., Zhang, H., Henry, C.E., Franklin, F.C.H., and Bomblies, K. (2020). Derived alleles of two axis proteins affect meiotic traits in autotetraploid *Arabidopsis arenosa*. Proc. Natl. Acad. Sci. USA *117*, 8980–8988.

41. Charles, D.R. (1938). The spatial distribution of cross-overs in X-chromosome tetrads of Drosophila Melanogaster. J. Genet. *36*, 103.

42. Zhang, L., Liang, Z., Hutchinson, J., and Kleckner, N. (2014). Crossover patterning by the beam-film model: analysis and implications. PLoS Genet. *10*, e1004042.

43. Loidl, J. (1986). Synaptonemal complex spreading in *Allium*. II. Tetraploid *A. vineale*. Can. J. Genet. Cytol. *28*, 754–761.

44. Jones, G.H., and Vincent, J.E. (1994). Meiosis in allopolyploid Crepis capillaris. II. Autotetraploids. Genome *37*, 497–505.

45. Rasmussen, S.W. (1987). Chromosome pairing in autotetraploid Bombyx males. Inhibition of multivalent correction by crossing over. Carlsberg Res. Commun. *52*, 211–242.

46. Stack, S.M., and Roelofs, D. (1996). Localized chiasmata and meiotic nodules in the tetraploid onion Allium porrum. Genome *39*, 770–783.

47. Humphrey, L.M. (1934). The meiotic divisions of haploid, diploid and tetraploid tomatoes with special reference to the prophase. Cytologia *5*, 278–300_1.

48. Higgins, J.D., Sanchez-Moran, E., Armstrong, S.J., Jones, G.H., and Franklin, F.C. (2005). The Arabidopsis synaptonemal complex protein ZYP1 is required for chromosome synapsis and normal fidelity of crossing over. Genes Dev. *19*, 2488–2500.

49. Higgins, J.D., Armstrong, S.J., Franklin, F.C., and Jones, G.H. (2004). The Arabidopsis MutS homolog AtMSH4 functions at an early step in recombination: evidence for two classes of recombination in Arabidopsis. Genes Dev. *18*, 2557–2570.

50. Chen, C., Zhang, W., Timofejeva, L., Gerardin, Y., and Ma, H. (2005). The Arabidopsis ROCK-N-ROLLERS gene encodes a homolog of the yeast ATP-dependent DNA helicase MER3 and is required for normal meiotic crossover formation. Plant J. *43*, 321–334.

51. Chelysheva, L., Gendrot, G., Vezon, D., Doutriaux, M.P., Mercier, R., and Grelon, M. (2007). Zip4/Spo22 is required for class I CO formation but not for synapsis completion in Arabidopsis thaliana. PLoS Genet. *3*, e83.

52. France, M.G., Enderle, J., Röhrig, S., Puchta, H., Franklin, F.C.H., and Higgins, J.D. (2021). ZYP1 is required for obligate cross-over formation and cross-over interference in *Arabidopsis*. Proc. Natl. Acad. Sci. USA *118*, e2021671118.

53. Hunter, N. (2015). Meiotic recombination: the essence of heredity. Cold Spring Harb. Perspect. Biol. *7*, a016618.

54. Terasawa, M., Ogawa, H., Tsukamoto, Y., Shinohara, M., Shirahige, K., Kleckner, N., and Ogawa, T. (2007). Meiotic recombination-related DNA synthesis and its implications for cross-over and non-cross-over recombinant formation. Proc. Natl. Acad. Sci. USA *104*, 5965–5970.

55. Alleva, B., and Smolikove, S. (2017). Moving and stopping: regulation of chromosome movement to promote meiotic chromosome pairing and synapsis. Nucleus *8*, 613–624.

56. López, E., Pradillo, M., Romero, C., Santos, J.L., and Cuñado, N. (2008). Pairing and synapsis in wild type Arabidopsis thaliana. Chromosome Res. *16*, 701–708.

57. Albini, S.M., and Jones, G.H. (1987). Synaptonemal complex spreading in *Allium cepa* and *A. fistulosum*. Chromosoma *95*, 324–338.

58. Pelé, A., Rousseau-Gueutin, M., and Chèvre, A.M. (2018). Speciation success of polyploid plants closely relates to the regulation of meiotic recombination. Front. Plant Sci. *9*, 907.

59. Bishop, D.K., and Zickler, D. (2004). Early decision; meiotic crossover interference prior to stable strand exchange and synapsis. Cell *117*, 9–15.

60. Caryl, A.P., Armstrong, S.J., Jones, G.H., and Franklin, F.C. (2000). A homologue of the yeast HOP1 gene is inactivated in the Arabidopsis meiotic mutant asy1. Chromosoma *109*, 62–71.

61. Ferdous, M., Higgins, J.D., Osman, K., Lambing, C., Roitinger, E., Mechtler, K., Armstrong, S.J., Perry, R., Pradillo, M., Cuñado, N., and Franklin, F.C. (2012). Inter-homolog crossing-over and synapsis in Arabidopsis meiosis are dependent on the chromosome axis protein AtASY3. PLoS Genet. *8*, e1002507.

62. Lambing, C., Kuo, P.C., Tock, A.J., Topp, S.D., and Henderson, I.R. (2020). ASY1 acts as a dosage-dependent antagonist of telomere-led recombination and mediates crossover interference in *Arabidopsis*. Proc. Natl. Acad. Sci. USA *117*, 13647–13658.

63. Viera, A., Berenguer, I., Ruiz-Torres, M., Gómez, R., Guajardo, A., Barbero, J.L., Losada, A., and Suja, J.A. (2020). PDS5 proteins regulate the length of axial elements and telomere integrity during male mouse meiosis. EMBO Rep. *21*, e49273.

64. Pradillo, M., Knoll, A., Oliver, C., Varas, J., Corredor, E., Puchta, H., and Santos, J.L. (2015). Involvement of the cohesin cofactor PDS5 (SPO76) during meiosis and DNA repair in Arabidopsis thaliana. Front. Plant Sci. *6*, 1034.

65. Bhatt, A.M., Lister, C., Page, T., Fransz, P., Findlay, K., Jones, G.H., Dickinson, H.G., and Dean, C. (1999). The DIF1 gene of Arabidopsis is required for meiotic chromosome segregation and belongs to the REC8/RAD21 cohesin gene family. Plant J. *19*, 463–472.

66. Tessé, S., Bourbon, H.M., Debuchy, R., Budin, K., Dubois, E., Liangran, Z., Antoine, R., Piolot, T., Kleckner, N., Zickler, D., and Espagne, E. (2017). Asy2/Mer2: an evolutionarily conserved mediator of meiotic recombination, pairing, and global chromosome compaction. Genes Dev. *31*, 1880–1893.

67. Capilla-Pérez, L., Durand, S., Hurel, A., Lian, Q., Chambon, A., Taochy, C., Solier, V., Grelon, M., and Mercier, R. (2021). The synaptonemal complex imposes crossover interference and heterochiasmy in *Arabidopsis*. Proc. Natl. Acad. Sci. USA *118*, e2023613118.

68. Dubois, E., De Muyt, A., Soyer, J.L., Budin, K., Legras, M., Piolot, T., Debuchy, R., Kleckner, N., Zickler, D., and Espagne, E. (2019). Building bridges to move recombination complexes. Proc. Natl. Acad. Sci. USA *116*, 12400–12409.

69. Armstrong, K.C. (1980). The cytology of tetraploid "*Bromus inermis*" and the C_o colchicine-induced octoploid. Can. J. Bot. *58*, 582–587.

70. Jenczewski, E., Eber, F., Grimaud, A., Huet, S., Lucas, M.O., Monod, H., and Chèvre, A.M. (2003). PrBn, a major gene controlling homeologous pairing in oilseed rape (Brassica napus) haploids. Genetics *164*, 645–653.

71. Sutton, T., Whitford, R., Baumann, U., Dong, C., Able, J.A., and Langridge, P. (2003). The Ph2 pairing homoeologous locus of wheat (Triticum aestivum): identification of candidate meiotic genes using a comparative genetics approach. Plant J. *36*, 443–456.

72. Rey, M.D., Martín, A.C., Higgins, J., Swarbreck, D., Uauy, C., Shaw, P., and Moore, G. (2017). Exploiting the *ZIP4* homologue within the wheat *Ph1* locus has identified two lines exhibiting homoeologous crossover in wheat-wild relative hybrids. Mol. Breed. *37*, 95.

73. Riley, R., and Chapman, V. (1958). Genetic control of the cytologically diploid behaviour of hexaploid wheat. Nature *182*, 713–715.

74. Mello-Sampayo, T. (1971). Genetic regulation of meiotic chromosome pairing by chromosome 3D of Triticum aestivum. Nat. New Biol. *230*, 22–23.

75. Sears, E.R. (1976). Genetic control of chromosome pairing in wheat. Annu. Rev. Genet. *10*, 31–51.

76. Sidhu, G.K., Rustgi, S., Shafqat, M.N., von Wettstein, D., and Gill, K.S. (2008). Fine structure mapping of a gene-rich region of wheat carrying Ph1, a suppressor of crossing over between homoeologous chromosomes. Proc. Natl. Acad. Sci. USA *105*, 5815–5820.

77. Armstrong, S.J., Caryl, A.P., Jones, G.H., and Franklin, F.C. (2002). Asy1, a protein required for meiotic chromosome synapsis, localizes to axis-associated chromatin in Arabidopsis and Brassica. J. Cell Sci. *115*, 3645–3655.

78. Lambing, C., Osman, K., Nuntasoontorn, K., West, A., Higgins, J.D., Copenhaver, G.P., Yang, J., Armstrong, S.J., Mechtler, K., Roitinger, E., and Franklin, F.C. (2015). Arabidopsis PCH2 mediates meiotic chromosome remodeling and maturation of crossovers. PLoS Genet. *11*, e1005372.

79. Schindelin, J., Arganda-Carreras, I., Frise, E., Kaynig, V., Longair, M., Pietzsch, T., Preibisch, S., Rueden, C., Saalfeld, S., Schmid, B., et al. (2012). Fiji: an open-source platform for biological-image analysis. Nat. Methods *9*, 676–682.

80. Longair, M.H., Baker, D.A., and Armstrong, J.D. (2011). Simple Neurite Tracer: open source software for reconstruction, visualization and analysis of neuronal processes. Bioinformatics *27*, 2453–2454.

81. Higgins, J.D., Wright, K.M., Bomblies, K., and Franklin, F.C. (2014). Cytological techniques to analyze meiosis in Arabidopsis arenosa for investigating adaptation to polyploidy. Front. Plant Sci. *4*, 546.

82. Morgan, C., and Wegel, E. (2020). Cytological characterization of Arabidopsis arenosa polyploids by SIM. Methods Mol. Biol. *2061*, 37–46.

83. Liu, H., Huang, J., Sun, X., Li, J., Hu, Y., Yu, L., Liti, G., Tian, D., Hurst, L.D., and Yang, S. (2018). Tetrad analysis in plants and fungi finds large differences in gene conversion rates but no GC bias. Nat. Ecol. Evol. *2*, 164–173.

84. Wijnker, E., Velikkakam James, G., Ding, J., Becker, F., Klasen, J.R., Rawat, V., Rowan, B.A., de Jong, D.F., de Snoo, C.B., Zapata, L., et al. (2013). The genomic landscape of meiotic crossovers and gene conversions in Arabidopsis thaliana. eLife *2*, e01426.

85. Higgins, J.D., Vignard, J., Mercier, R., Pugh, A.G., Franklin, F.C., and Jones, G.H. (2008). AtMSH5 partners AtMSH4 in the class I meiotic crossover pathway in Arabidopsis thaliana, but is not required for synapsis. Plant J. *55*, 28–39.

86. Crismani, W., Girard, C., Froger, N., Pradillo, M., Santos, J.L., Chelysheva, L., Copenhaver, G.P., Horlow, C., and Mercier, R. (2012). FANCM limits meiotic crossovers. Science *336*, 1588–1590.

STAR★METHODS

KEY RESOURCES TABLE

REAGENT or RESOURCE	SOURCE	IDENTIFIER
Antibodies		
Rat polyclonal anti-ASY1	Armstrong et al.[77]	N/A
Guinea-pig polyclonal anti-ZYP1	Higgins et al.[48]	N/A
Rabbit polyclonal anti-HEI10	Lambing et al.[78]	N/A
Goat anti-rat Alexa Fluor 555 (F(ab')2 fragment)	Abcam	Cat#: ab150162
Goat anti-guinea-pig Alexa Fluor 488	Thermofisher	RRID: AB_2534117
Goat anti-rabbit Alexa Fluor 647 (F(ab')2 fragment)	Thermofisher	RRID: AB_2535814
Chemicals, peptides, and recombinant proteins		
Colchicine	Sigma-Aldrich	Cat#: C3915
Cellulase	Sigma-Aldrich	Cat#: C1794
Pectolyase	Sigma-Aldrich	Cat#: P5936
4',6-diamidino-2-phenylindole (DAPI)	Thermofisher	Cat#: D1306
Vectashield mounting medium	2bscientific	Cat#: H-1000-1
Cytohelicase	Sigma-Aldrich	Cat#: C8274
Polyvinylpyrrolidone	Sigma-Aldrich	Cat#: PVP40
Lipsol	Appleton Woods	Cat#: LP40023
Triton X-100	Sigma-Aldrich	Cat#: X100
Paraformaldehyde	Fisher Scientific	Cat#: 114090570
200 nm TetraSpeck microspheres	Thermofisher	Cat#: T7280
Deposited data		
3D-SIM imaging data	This paper	https://doi.org/10.3929/ethz-b-000470079
Component homolog measurements	This paper	https://doi.org/10.17632/zn23pxwgz3.1
Experimental models: Organisms/strains		
Arabidopsis arenosa – Streçno accession	Collected from wild populations[28]	N/A
Arabidopsis arenosa – Triberg accession	Collected from wild populations[28]	N/A
Arabidopsis arenosa – Kasparstein accession	Collected from wild populations[28]	N/A
Software and algorithms		
Zen – Elyra PS1 2012	Zeiss	https://www.zeiss.com/microscopy/int/home.html
ImageJ – Version 2.1.0/1.53c	Schindelin et al.[79]	https://imagej.nih.gov/ij/
Simple Neurite Tracer Version 3.2.5	Longair et al.[80]	https://fiji.sc/Simple_Neurite_Tracer
MATLAB v2020b	Mathworks	R2020b
EvolvingStablePolyploidy v1.0.0 (custom MATLAB analysis code)	This paper	https://doi.org/10.5281/zenodo.5033552

RESOURCE AVAILABILITY

Lead contact

Further information and requests for resources and reagents should be directed to and will be fulfilled by the lead contact, Kirsten Bomblies (kirsten.bomblies@biol.ethz.ch).

Materials availability

The only unique reagents generated in this study are the neo-polyploid lines, but these are not genetically stable and cannot be propagated, and thus are not available for distribution. This study did not generate any other new unique reagents.

Data and code availability

- Microscopy data has been deposited at the ETH research collection and is publicly available as of the date of publication. The DOI is listed in the Key resources table. Primary component homolog measurements have been deposited at Mendeley and are publicly available as of the date of publication. The DOI is listed in the Key resources table.
- All original code has been deposited at Zenodo and is publicly available as of the date of publication. DOIs are listed in the Key resources table.
- Any additional information required to reanalyze the data reported in this paper is available from the lead contact upon request.

EXPERIMENTAL MODEL AND SUBJECT DETAILS

For diploid *A. arenosa,* we used a line originally collected from Streçno, Slovakia (SN; 49.17417N, 18.86167E) and for the established tetraploid we used a line originally collected from Triberg, Germany (TBG; 48.13972N, 8.23667E) and another originally collected from Kasparstein, Austria (KA; 46.68833N, 14.87167E).[28] Plants were grown in controlled environment rooms with 16 h of light (125 μmol m^2 s^{-1}, cool white) at 20°C, and 8 h of dark at 16°C. *A. arenosa* is hermaphroditic. Male meiocytes were used exclusively in this investigation.

METHOD DETAILS

Plant Material

To generate neo-polyploid plants, we treated plants with colchicine. In brief, 3 weeks after sowing, when plants were at the rosette stage of growth, 20 μL of 0.25% colchicine solution was pipetted into the center of the rosette. The flowering stems that emerged from treated plants were screened cytologically for polyploidization. In some instances, both diploid and neo-tetraploid stems were produced by the same diploid progenitor plant, with diploid stems providing valuable control material to ensure colchicine treatment had no direct effects on meiosis. Meiocytes were gathered from four independent diploid, neo-tetraploid and established tetraploid plants. The two neo-octoploid plants were independently generated by colchicine treatment of a single diploid and a single established tetraploid plant. Plant fertility was not assayed in this study.

Metaphase I Spreads

For metaphase spreads, we followed a previously described protocol.[81,82] Briefly, we fixed inflorescences in 3:1 ethanol: acetic acid. Anthers were isolated and subsequently incubated in 300 μl of enzyme mixture (0.3% cellulase, 0.3% pectolyase in 10 mM citrate buffer) in a most chamber at 37°C for 90 minutes. Two buds were transferred to 2 μl of 80% acetic acid on a slide and macerated with a brass-rod. 10 μl of 80% acetic acid was then added to the slide, and the slide was placed on a 45°C hot block for 30 s, before adding another 10 μl of 80% acetic acid and leaving the slide on the hot-block for another 30 s. 2 × 200 μl of 3:1 fixative was then added to the slide, before drying the back of the slide with a hairdryer. Slides were then mounted in 7 μl 1 μg/ml 4',6-diamidino-2-phenylindole (DAPI) in Vectashield mounting medium (Vector Laboratories). All images are available via the ETH data repository: https://doi.org/10.3929/ethz-b-000470079

Immunocytology

For immunostaining of *A. arenosa* pachytene cells, we followed described protocols.[40,82] Briefly, anthers containing meiocytes of the desired stage were dissected from fresh buds and macerated on a No. 1.5H coverslip (Marienfeld) in 10 μl digestion medium (0.4% cytohelicase (Sigma), 1.5% sucrose, 1% polyvinylpyrrolidone (Sigma) in sterile water) for 1 minute using a brass rod. Coverslips were then incubated in a moist chamber at 37°C for 4 minutes before adding 10 μl of 2% Lipsol solution (SciLabware) followed by 20 μl 4% paraformaldehyde (pH 8). Once coverslips were dry, they were blocked in 0.3% BSA in PBS and then incubated with primary antibody overnight at 4°C and secondary antibody for 2 hr at 37°C. Before and after each antibody incubation coverslips were washed in 1 X PBS solution plus 0.1% Triton X-100 (Sigma). Coverslips were finally incubated in 10 μg/ml 4',6-diamidino-2-phenylindole (DAPI) for 5 minutes before being mounted on a slide in 7 μl Vectashield (Vector Laboratories). The following primary antibodies were used at 1:500 dilutions: rat polyclonal anti-ASY1, guinea-pig polyclonal anti-ZYP1, rabbit polyclonal anti-HEI10. The following secondary antibodies were used at 1:200 dilutions: goat anti-rat Alexa Fluor 555 (F(ab')2 fragment, Abcam), goat anti-guinea-pig Alexa Fluor 488 (Thermofisher), goat anti-rabbit Alexa Fluor 647 (F(ab')2 fragment, Thermofisher). Immunostained cells were imaged using 4-color structured illumination microscopy (3D-SIM) on a Zeiss Elyra PS1 microscope equipped with an EM-CCD camera, a Plan-Apochromat 63x, NA 1.40 oil objective and 405, 488, 561 and 642 nm solid state laser diodes. Slides were imaged in 3D SIM mode with three stripe angles and five phases according to the microscope manufacturer's instructions. Z stacks were captured at an interval size of 0.0909 μm, with the size of each stack being sufficiently large for the cell to be out of focus at both ends. An immersion oil with a refractive index of 1.515 was used that was optimized for the green/red (ZYP1/ASY1) channels of our system. To determine the best refractive index, 200 nm TetraSpeck microspheres (Invitrogen) were dried on a coverslip at 1/100 dilution, mounted on a slide in 7 μL Vectashield, imaged using the same microscope settings as used for the experiments and then the symmetry of the PSFs for each channel was assessed in orthogonal sections through the stack. Channel alignment was performed using the same Tetraspeck

beads and the 'affine' alignment algorithm that is included in the Zeiss Elyra software Zen. All images are available via the ETH data repository: https://doi.org/10.3929/ethz-b-000470079

QUANTIFICATION AND STATISTICAL ANALYSIS

The statistical details of experiments can be found in the corresponding Figure legends. The results of statistical tests can be found in the corresponding Results section. Statistical tests were carried out using MATLAB v2020b.

Sample Sizes

For examination of phenotypes at metaphase I, the following number of meiocytes were examined: 126 diploid meiocytes of a single plant, 83 neo-tetraploid meiocytes from two plants (39 and 44 meiocytes each), 353 established tetraploid meiocytes from four plants (51, 55, 99 and 148 meiocytes each), 107 diploid-derived-neo-octoploid meiocytes from a single plant and 137 established tetraploid-derived-neo-octoploid meiocytes from a single plant. All examined meiocytes exhibited the same appearances as shown in Figures 1 and 7.

For analysis of pachytene phenotypes, meiocytes were gathered from four independent diploid, neo-tetraploid and established tetraploid plants. Material from one colchicine treated mosaic plant with both diploid and neo-tetraploid stems was used for both diploid and neo-tetraploid datasets (11 plants total). A total of 90 nuclei were examined from the four diploid plants. Since *A. arenosa* possesses eight genetic chromosomes, this gave measurements for a total of (90 × 8 x 2) 1,440 component homologs. A total of 9, 17, 22 and 42 nuclei (or 144, 272, 352 and 672 component homologs) were examined for the four different plants. A total of 43 nuclei were examined from the four neo-tetraploid plants providing measurements for a total of (43 × 8 x 4) 1,376 component homologs. A total of 10, 10, 10 and 13 nuclei (or 320, 320, 1320, 416 component homologs) were examined for the four different plants. A total of 61 nuclei were examined from the four established tetraploid plants providing measurements for a total of (61 × 8 x 4) 1,952 component homologs. At total of 13, 15, 16 and 17 nuclei (or 416, 480, 512, 544 component homologs) were examined for the four different plants. For the neo-octoploids, 32 nuclei were examined from a single diploid-derived plant, and 47 nuclei were examined from a single tetraploid-derived plant,

Defining synapsis patterns and CO positions

CO patterns were defined by cytological analysis of prophase nuclei at the late pachytene stage, where SC is full length and CO sites are specifically marked by prominent SC-associated recombination complexes. We visualized four different chromosomal components simultaneously by immunofluorescence 3D SIM imaging of spread nuclei that still retain significant 3D character (Figures 2A and S1A; Video S1). SC paths were defined via the primary SC central-region component ZYP1,[48] and CO recombination complexes along these SCs via foci of the diagnostic E3 ligase HEI10, which is known to mark the sites of COs in a variety of organisms (reviewed in Hunter[53]). By analogy with *A. thaliana*, there may exist 10%–15% more genetic COs than are detected by HEI10 foci, i.e., "Class II" COs,[67,83–85] which could potentially contribute to metaphase I multivalents in both tetraploids.[86] However, the good correspondence between pachytene HEI10-marked Class I CO patterns and metaphase I chiasmata patterns in *A. arenosa* indicate that this contribution is minor[40] (Figure S3). We also imaged HORMAD protein ASY1 (Hop1), a major component of individual homolog axes,[60] because bright ASY1 staining specifically identifies regions where SC has failed to form ("asynapsis"; Figure 2A yellow arrowhead). Finally, bulk DNA/chromatin was visualized by DAPI staining (Figure S1). The paths of all SCs were traced along their lengths by ImageJ Simple Neurite Tracer plugin[80] (Figure 2B). SC configurations were then segmented into individual units, i.e., bivalents in diploids, and bivalents or quadrivalents in tetraploids. The positions of associated HEI10/CO recombination complexes, and regions of asynapsis along the SC paths, were then defined (Figure 2C).

Component Homolog Generation

Component homolog measurements were derived from image measurements using the custom MATLAB function generateComponentHomologs of EvolvingStablePolyploidy v1.0.0. Briefly, to circumvent potential measurement bias, the left/right orientation of each pachytene bivalent and quadrivalent was first randomized. Then, for each pachytene bivalent, its two component homologs are simple duplicates of the image measurement. For each pachytene quadrivalent, the measurements of each of its four component homologs was derived by switching one of each paired homolog at each SPS site as described above (Figure 3A). In this manner, for pachytene quadrivalents with a single SPS, the measurements of each component homolog can be unambiguously defined. This is not the case for pachytene quadrivalents with more than one SPS. However, such cases were rare and multiple independent runs of the component homolog generation software with randomized component homolog switching at SPSs were used to confirm that conclusions were robust to this unknown (Figure S2). Unless otherwise stated, the component homologs of individual plants were aggregated. Component homolog measurements are available from Mendeley data: https://doi.org/10.17632/zn23pxwgz3.1

Coefficient of Coincidence Analysis

Co-efficient of coincidence was calculated by dividing component homologs of total SC length ranging between 27 and 33 μm into 18 equally sized intervals using the custom MATLAB function generateLengthBinnedCoC of EvolvingStablePolyploidy v1.0.0. This specific range of homolog lengths was used as it is representative of diploid, neo-tetraploid and established tetraploid homolog lengths

and is longer than the interference distance (Figure 4A). Analysis of homologs of different length ranges gave comparable results (Figure S4A). Pachytene bivalents were excluded from the analysis when calculating the coefficient of coincidence analysis of SPS sites (Figure 6B). Coefficient of Coincidence values for 2-homolog and 3-homolog double COs were calculated using the custom MATLAB function generate2H3HLengthBinnedCoC of EvolvingStablePolyploidy v1.0.0. Expected double CO frequencies were calculated using all data (single CO homologs, 2-homolog double CO homologs and 3-homolog double CO homologs). Observed double CO frequencies were normalized to the observed double CO frequencies of all double COs to account for 2-homolog double CO bias (Figure 6G).

Current Biology, Volume *31*

Supplemental Information

Evolution of crossover interference enables stable autopolyploidy by ensuring pairwise partner connections in *Arabidopsis arenosa*

Chris Morgan, Martin A. White, F. Chris H. Franklin, Denise Zickler, Nancy Kleckner, and Kirsten Bomblies

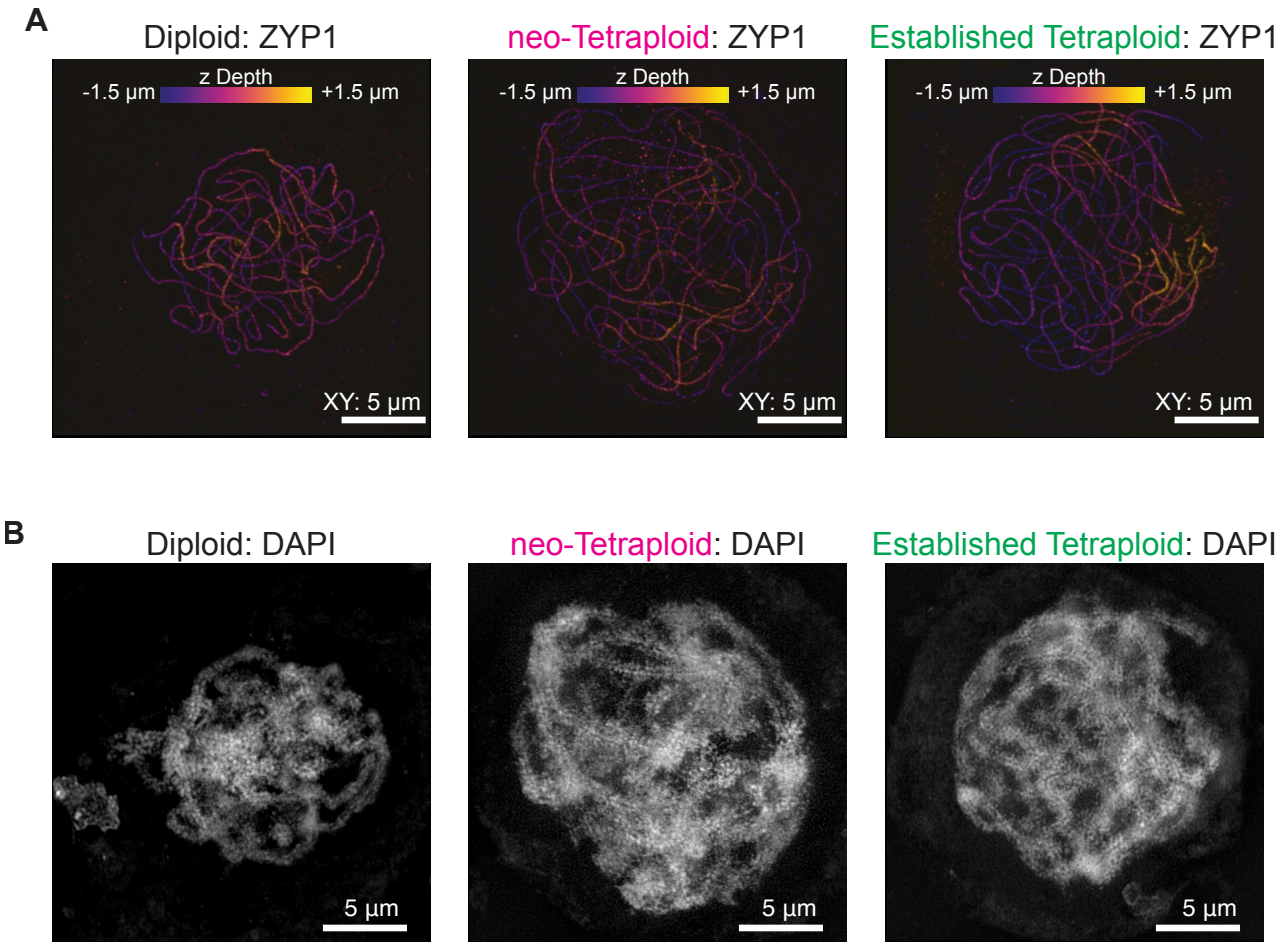

Figure S1. Additional 3D immunofluorescence SIM images of *A. arenosa* diploid, neo-tetraploid and established tetraploid late pachytene nuclei. Related to Figure 2 and Video S1.

A. Mildly squashed pachytene nuclei still retain significant 3D character. Maximum intensity z-projections of ZYP1 images of pachytene diploid, neo-tetraploid and established tetraploid nuclei presented in Figure 2, color coded for z-depth. Scale bars show 5 µm.

B. DAPI images showing the DNA of the pachytene diploid, neo-tetraploid and established tetraploid nuclei presented in Figure 2. Scale bars show 5 µm.

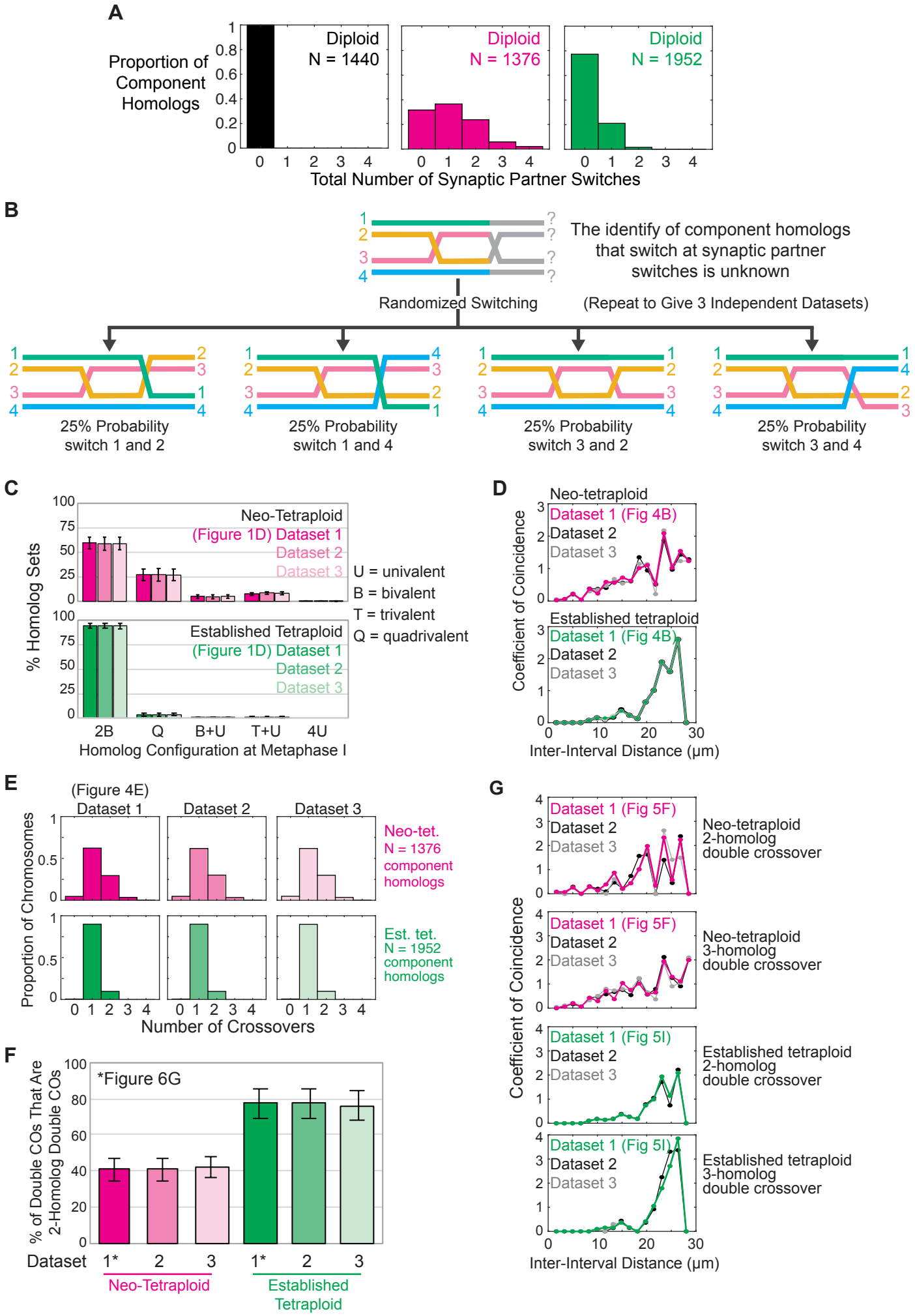
A
Proportion of Component Homologs
Diploid N = 1440
Diploid N = 1376
Diploid N = 1952
Total Number of Synaptic Partner Switches
B
The identify of component homologs that switch at synaptic partner switches is unknown
Randomized Switching
(Repeat to Give 3 Independent Datasets)
25% Probability switch 1 and 2
25% Probability switch 1 and 4
25% Probability switch 3 and 2
25% Probability switch 3 and 4
C
% Homolog Sets
Neo-Tetraploid (Figure 1D) Dataset 1
Dataset 2
Dataset 3
Established Tetraploid (Figure 1D) Dataset 1
Dataset 2
Dataset 3
U = univalent
B = bivalent
T = trivalent
Q = quadrivalent
2B
Q
B+U
T+U
4U
Homolog Configuration at Metaphase I
D
Neo-tetraploid
Established tetraploid
Dataset 1 (Fig 4B)
Dataset 2
Dataset 3
Coefficient of Coincidence
Inter-Interval Distance (μm)
E
(Figure 4E)
Dataset 1
Dataset 2
Dataset 3
Proportion of Chromosomes
Neo-tet. N = 1376 component homologs
Est. tet. N = 1952 component homologs
Number of Crossovers
F
*Figure 6G
% of Double COs That Are 2-Homolog Double COs
Dataset
Neo-Tetraploid
Established Tetraploid
G
Dataset 1 (Fig 5F)
Dataset 1 (Fig 5I)
Neo-tetraploid 2-homolog double crossover
Neo-tetraploid 3-homolog double crossover
Established tetraploid 2-homolog double crossover
Established tetraploid 3-homolog double crossover
Coefficient of Coincidence
Inter-Interval Distance (μm)

Figure S2. Randomized switching of component homologs at synaptic partner switches. Related to Figure 1, Figure 3, Figure 4, Figure 5 and Figure 6.

A. Distribution of number of synaptic partner switches per component homolog.

B. Component homologs of pachytene quadrivalents with two or more synaptic partner switches cannot be unambiguously defined. For each pachytene quadrivalent, one of each paired component homolog was randomly chosen to switch partners. Three independent component homolog datasets were generated in such a manner for both the neo- and established tetraploid to test the impact of this unknown on measurements.

C. Predicted metaphase I configurations of total homolog sets for each of the three independent component homolog datasets for *A. arenosa* neo-tetraploid and established tetraploid nuclei as defined by component homolog analysis of crossovers along pachytene chromosomes. Error bars show standard error of the mean, N = 4 plants for both neo-tetraploid and established tetraploid.

D. Coefficient of coincidence analysis for each of the three independent component homolog datasets for *A. arenosa* neo-tetraploids and established tetraploids. N = 486 and 622 component homologs between 27 and 33 μm in length for neo-tetraploid and established tetraploid respectively.

E. Distribution of numbers of crossovers per component homolog for each of the three independent component homolog datasets for *A. arenosa* neo-tetraploids and established tetraploids.

F. The percentage of observed double crossovers that are two-homolog double crossovers for each of the three independent component homolog datasets for *A. arenosa* neo-tetraploids and established tetraploids. Error bars show standard error of the mean, N = 4 plants for neo-tetraploid and established tetraploid.

G. Coefficient of coincidence analysis for 2-homolog and 3-homolog double crossovers for each of the three independent component homolog datasets for *A. arenosa* neo-tetraploids and established tetraploids. N = 486 and 622 component homologs between 27 and 33 μm in length for neo-tetraploid and established tetraploid respectively.

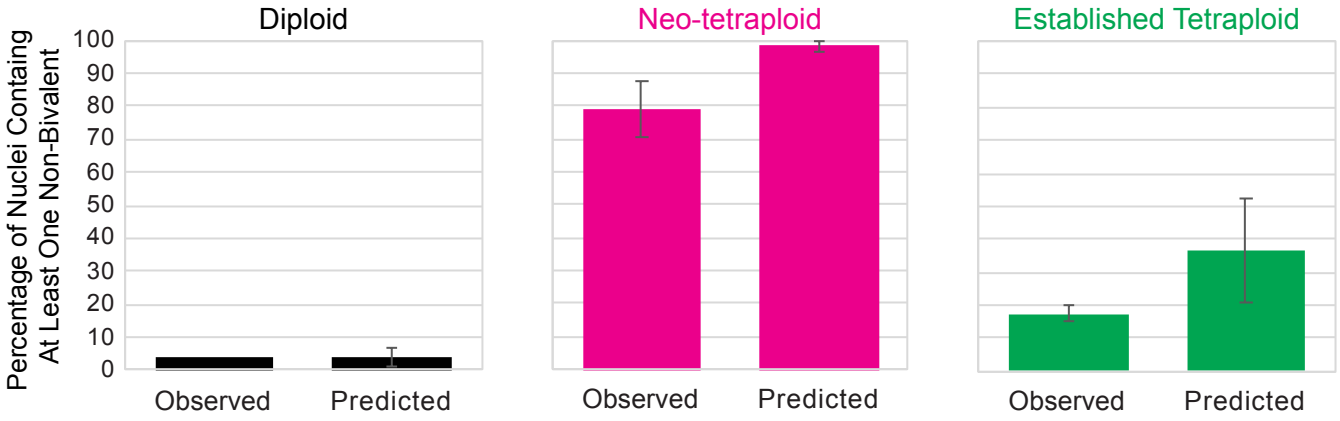

Figure S3. Observed and Predicted Metaphase I Patterns. Related to Figure 1. The observed percentage of nuclei with at least one non-bivalent structure (univalent or multivalent) and the percentage predicted from observed pachytene HEI10 foci patterns for diploid, neo-tetraploid and established tetraploid. Error bars show standard error of the mean. N = 1, 2, and 4 plants for observed diploid, neo-tetraploid and established tetraploid values. N = 4 plants for predicted values for diploid, neo-tetraploid and established tetraploid. No stastically signficant difference between observed and predicted values was obtained for diploid (p = 0.67), neo-tetraploid (p = 0.19), nor established tetraploid (p = 0.17); Wilcoxon rank sum test.

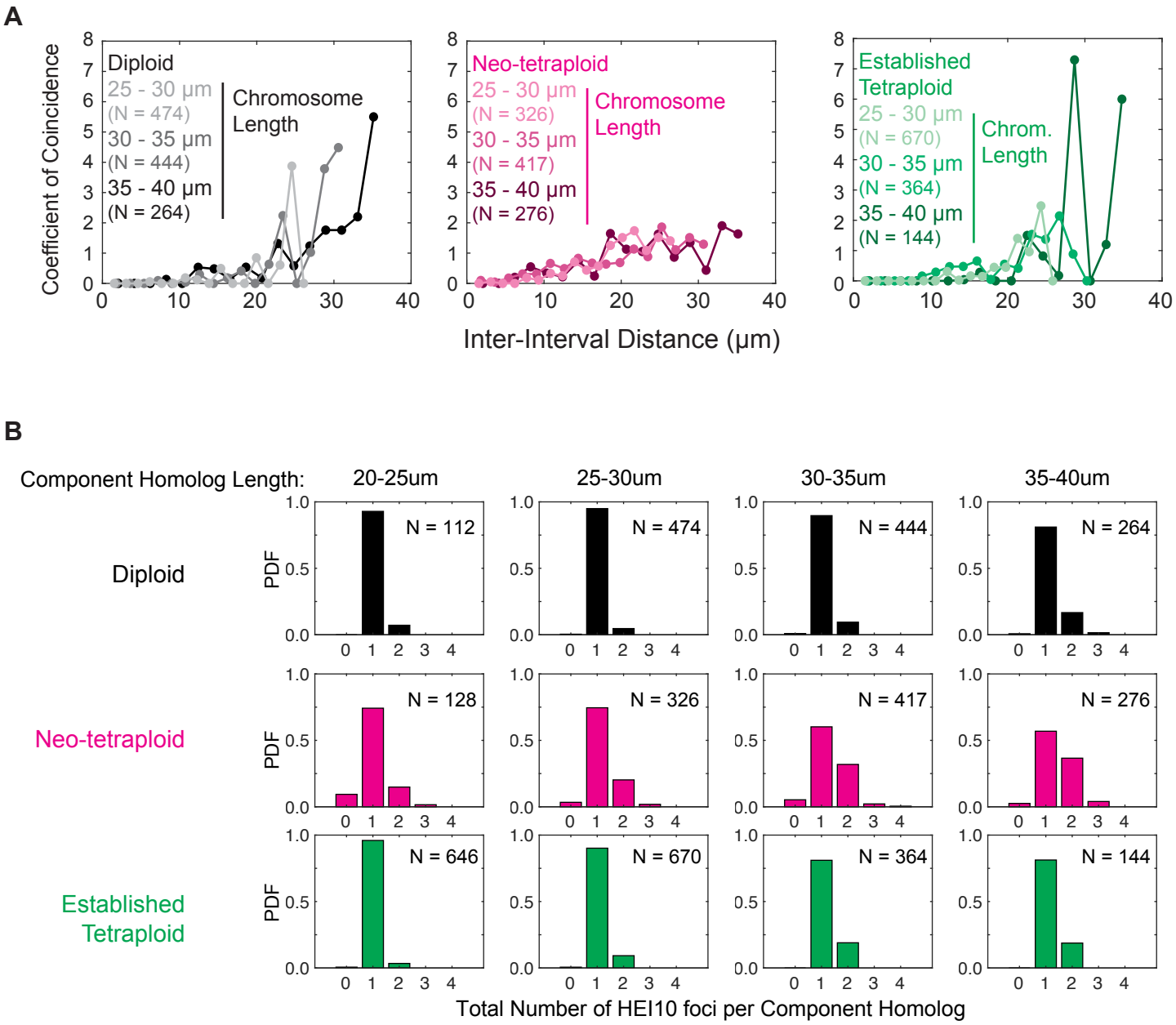

Figure S4. Component Homolog Length and Crossover Parameters. Related to Figure 4.
A. Coefficient of coincidence analysis of diploid, neo-tetraploid and established tetraploid component homologs of three different ranges of component homolog length.
B. The frequency of crossovers (HEI10 foci) on diploid, neo-tetraploid and established tetraploid component homologs of four different length bins.

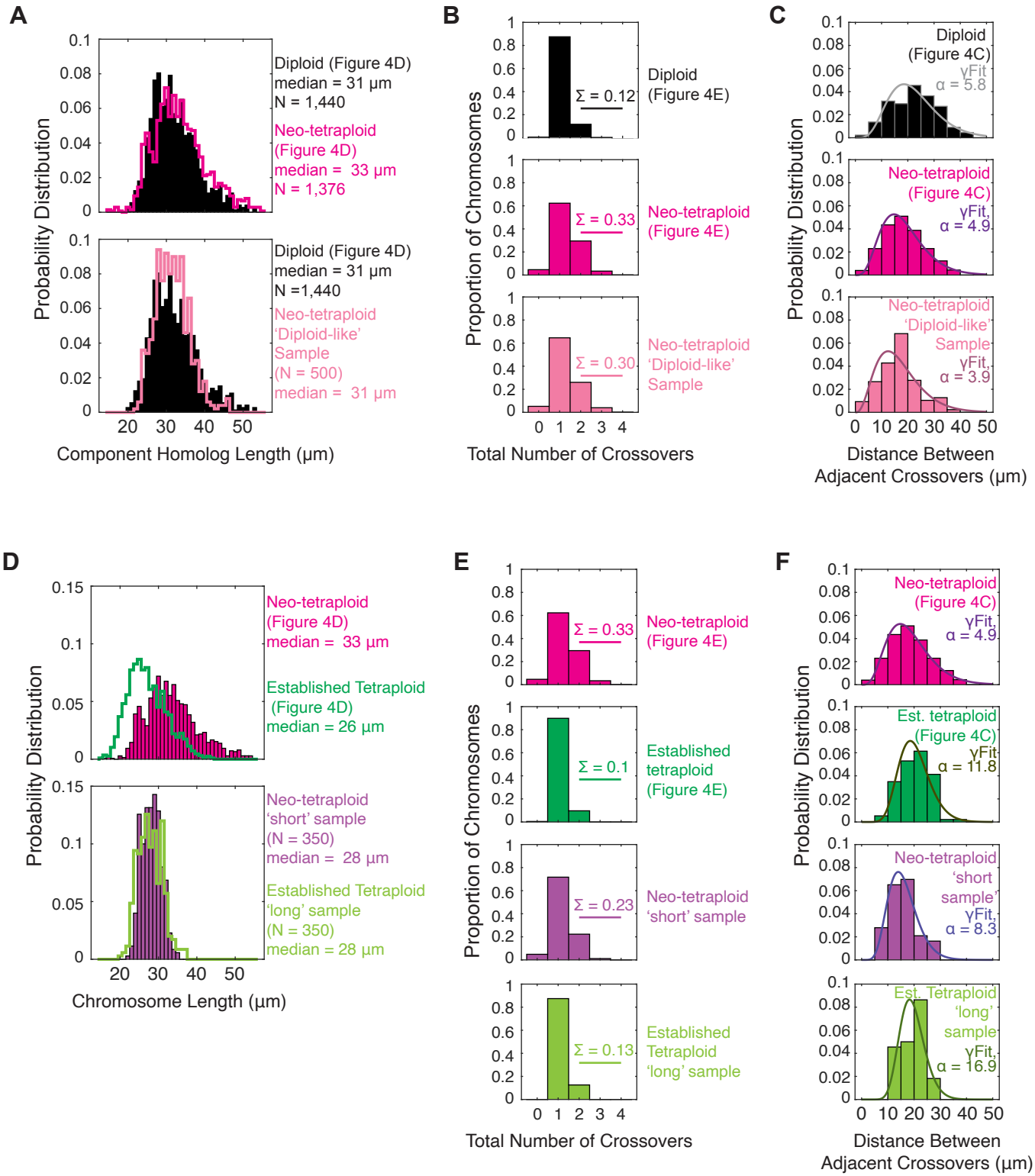
A
Probability Distribution
Component Homolog Length (μm)
Diploid (Figure 4D)
median = 31 μm
N = 1,440
Neo-tetraploid
(Figure 4D)
median = 33 μm
N = 1,376
Diploid (Figure 4D)
median = 31 μm
N =1,440
Neo-tetraploid
'Diploid-like'
Sample
(N = 500)
median = 31 μm
B
Proportion of Chromosomes
Total Number of Crossovers
Σ = 0.12
Diploid
(Figure 4E)
Σ = 0.33
Neo-tetraploid
(Figure 4E)
Σ = 0.30
Neo-tetraploid
'Diploid-like'
Sample
C
Probability Distribution
Distance Between
Adjacent Crossovers (μm)
Diploid
(Figure 4C)
γFit
α = 5.8
Neo-tetraploid
(Figure 4C)
γFit,
α = 4.9
Neo-tetraploid
'Diploid-like'
Sample
γFit,
α = 3.9
D
Probability Distribution
Chromosome Length (μm)
Neo-tetraploid
(Figure 4D)
median = 33 μm
Established Tetraploid
(Figure 4D)
median = 26 μm
Neo-tetraploid
'short' sample
(N = 350)
median = 28 μm
Established Tetraploid
'long' sample
(N = 350)
median = 28 μm
E
Proportion of Chromosomes
Total Number of Crossovers
Σ = 0.33
Neo-tetraploid
(Figure 4E)
Σ = 0.1
Established
tetraploid
(Figure 4E)
Σ = 0.23
Neo-tetraploid
'short' sample
Σ = 0.13
Established
Tetraploid
'long' sample
F
Probability Distribution
Distance Between
Adjacent Crossovers (μm)
Neo-tetraploid
(Figure 4C)
γFit,
α = 4.9
Est. tetraploid
(Figure 4C)
γFit
α = 11.8
Neo-tetraploid
'short
sample'
γFit,
α = 8.3
Est. Tetraploid
'long'
sample
γFit,
α = 16.9

Figure S5. The effect of changes in chromosome length on crossover counts. Related to Figure 4.

A, Although neo-tetraploids have, on average, longer chromosomes than diploids, the two distributions overlap significantly allowing a sub-sample of 500 neo-tetraploid component homologs with diploid-like lengths to be obtained using the custom MATLAB function generateMatchingLengthDistribution of program EvolvingStablePolyploidy v1.0.0. The crossover patterns of this diploid-like subsample of neo-tetraploid chromosomes were analyzed. The distribution of component homolog lengths are shown. For the diploid and neo-tetraploid 'diploid-like' samples, $p = 0.33$, Wilcoxon rank sum test.

B, distribution of numbers of crossovers per componemnt homolog with the sum of those with two or more crossovers indicated. For the diploid and neo-tetraploid 'diploid-like' samples, $p = 7 \times 10^{-13}$; Wilcoxon rank sum test.

C, distribution of distances between adjacent crossovers with shape parameter (α) of best-fit gamma distribution (γFit). For the diploid and neo-tetraploid 'diploid-like' samples, $p = 6 \times 10^{-10}$; Wilcoxon rank sum test.

D, a sample of 350 neo-tetraploid and 350 established tetraploid component homologs of comparable length were generated using the custom MATLAB function generateMatchingLengthDistribution (neo-tetraploid 'short' sample and established tetraploid 'long' sample respectively; $p = 0.12$; Wilcoxon rank sum test.

E, distribution of numbers of crossovers per component homolog with the sum of those with two or more crossovers indicated. For the neo-tetraploid 'short' sample and established tetraploid 'long' sample, $p = 0.02$; Wilcoxon rank sum test.

F, distribution of distances between adjacent crossovers with shape parameter (α) of best-fit gamma distribution (γFit). For the neo-tetraploid 'short' sample and established tetraploid 'long' sample, $p = 1 \times 10^{-4}$; Wilcoxon rank sum test.

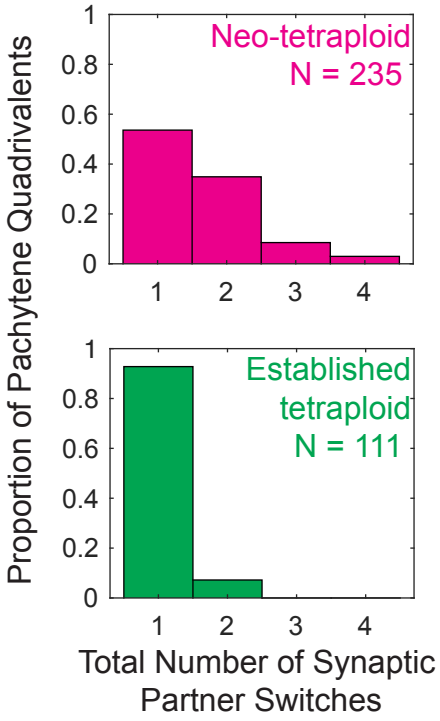

Figure S6. Distribution of total number of synaptic partner switches. Related to Figure 6. Distributions of total number of synaptic partner switches in pachytene quadrivalents.